

**A theoretical study of the atmospherically important
radical-radical reaction $\text{BrO} + \text{HO}_2$;
the product channel $\text{O}_2(\text{a}^1\Delta_{\text{g}}) + \text{HOBr}$ is formed with the highest rate.**

Ronald Chow ^[a], Daniel K.W. Mok ^[a], Edmond P. F. Lee ^{*[a],[b]}, and John M. Dyke ^{*[b]}

^[a] Department of Applied Biology and Chemical Technology, Hong Kong Polytechnic University, Hung Hom, Hong Kong

^[b] School of Chemistry, University of Southampton, Highfield, Southampton SO17 1BJ, United Kingdom e-mail epl@soton.ac.uk; jmdyke@soton.ac.uk

*addresses for correspondence

Abstract

A theoretical study has been made of the BrO + HO₂ reaction, a radical-radical reaction which contributes to ozone depletion in the atmosphere via production of HOBr. Reaction enthalpies, activation energies and mechanisms have been determined for five reaction channels. Also rate coefficients have been calculated, in the atmospherically important temperature range 200-400 K, for the two channels with the lowest activation energies, both of which produce HOBr:-

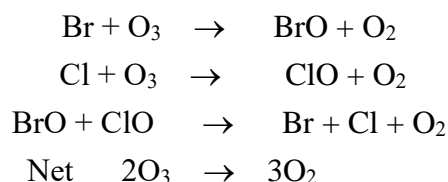
1(a) HOBr (X^1A') + O₂($X^3\Sigma^-_g$) and 1(b) HOBr (X^1A') + O₂($a^1\Delta_g$). The other channels considered are :- (2) BrO + HO₂ → HBr + O₃, (3) BrO + HO₂ → OBrO + OH and (4) BrO + HO₂ → BrOO + OH. For all channels, geometry optimization and frequency calculations were carried out at the M06-2X/AVDZ level, while relative energies of the stationary points on the reaction surface were improved at a higher level (BD(TQ)/CBS or CCSD(T)/CBS).

The computed standard reaction enthalpies (ΔH_{298K}^{RX}) for channels 1a, 1b, 2, 3 and 4 are -47.5, -25.0, -4.3, 14.9 and 5.9 kcal.mol⁻¹, and the corresponding computed activation energies (ΔE) are 2.53, -3.07, 11.83, 35.0 and 37.81 kcal.mol⁻¹. These values differ significantly from those obtained in earlier work by Kaltsoyannis and Rowley (PCCP 4, 2002, 419-427), particularly for channel 1(b), and reasons for this are discussed. In particular, the importance of obtaining an open-shell singlet wavefunction, rather than a closed-shell singlet wavefunction, for the transition state of this channel is emphasized.

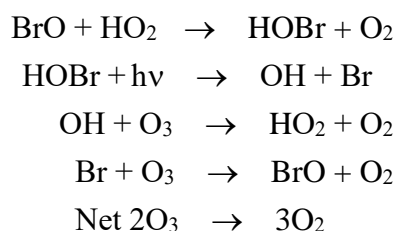
Rate coefficient calculations from computed potential energy surfaces were made for BrO + HO₂ for the first time. Although channel 1(a) is the most exothermic, channel 1(b) has the lowest barrier height, which is negative (at -3.07 kcal.mol⁻¹). Most rate coefficient calculations were therefore made for 1(b). A two transition state model has been used, involving an outer and an inner transition state. The inner transition state was found to be the major bottleneck of the reaction with the outer transition state having essentially no effect on the overall rate coefficient (k) in the temperature range considered. Studying the entropy, enthalpy and free energy of activation of this channel as a function of temperature shows that the main contributor to the magnitude of lnk at a selected temperature is the entropy term ($\Delta S^\ddagger/k_B$) whereas the temperature dependence of lnk is determined mainly by the enthalpy term ($-\Delta H^\ddagger/k_B T$). This compares with reactions with positive barrier heights where the enthalpy term makes a bigger contribution to lnk. Comparison of the computed rate coefficients with available experimental values shows that the computed values have a negative temperature dependence, as observed experimentally, but are too low by approximately an order of magnitude at any selected temperature in the range 200-400 K.

Introduction

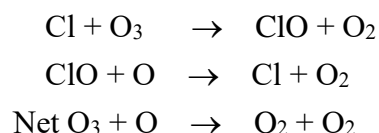
The BrO + HO₂ reaction is important in the earth's atmosphere as it can lead to enhanced destruction of ozone. In modelling studies, Yung et al.(1) concluded that the following catalytic cycle, which involves both bromine and chlorine atoms, is important in contributing to ozone depletion in the stratosphere:-



However, the BrO + HO₂ reaction also contributes to ozone depletion. This occurs through production of HOBr, which then undergoes solar photolysis, followed by reactions of the radicals produced with ozone:-



Important features of this cycle are that the BrO + HO₂ → HOBr + O₂ reaction is the rate limiting step, and that the cycle does not require the presence of atomic oxygen, as do the separate ozone-removal cycles involving chlorine and bromine atoms. For example, the key steps in the cycle involving removal of ozone by chlorine atoms are:-



Therefore, the BrO + HO₂ reaction is particularly relevant to ozone removal during the day in the lower stratosphere, where the concentration of atomic oxygen is low compared to higher regions of the stratosphere.

The value of the rate coefficient at 298 K of the BrO + HO₂ reaction used by Yung et al.(1) in their modelling studies in 1980 was $4 \times 10^{-12} \text{ cm}^3 \text{ molecule}^{-1} \text{ s}^{-1}$. This was taken to be equal to the measured value for the ClO + HO₂ reaction at that time, and it appeared to be confirmed when in 1982 Cox and Sheppard (2) measured the BrO + HO₂ rate coefficient as $5 \times 10^{-12} \text{ cm}^3 \cdot \text{molecule}^{-1} \text{ s}^{-1}$ using molecular modulation u.v. absorption spectroscopy to monitor both BrO and HO₂. However, more recent experimental studies (3-12) gave values for this rate coefficient at room temperature which are ~6 times higher (the recommended value at 298 K is currently $(2.4 \pm 0.8) \times 10^{-11} \text{ cm}^3 \text{ molecule}^{-1} \text{ s}^{-1}$ (3)). This higher value indicates that this reaction is more important than was first thought in ozone depletion. Also, measurements over the temperature range 210-360 K show that the rate coefficient increases when the temperature decreases (at 210 K the approximate temperature at

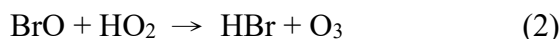
an altitude of 15 km, the start of the stratosphere, the rate coefficient is $4.87 \times 10^{-11} \text{ cm}^3 \text{ molecule}^{-1} \text{ s}^{-1}$) (3). This negative temperature dependence of the rate coefficient suggests that the reaction proceeds through a reactant complex (10).

In the $\text{BrO} + \text{HO}_2$ reaction, the ground electronic states of the reactants are doublets. The reaction can therefore take place on a triplet or a singlet surface {for example with production of $\text{HOBr} (X^1A') + \text{O}_2(X^3\Sigma^-_g)$ or $\text{HOBr} (X^1A') + \text{O}_2(a^1\Delta_g)$ }. For the singlet surface, the reactant complex (RC) and transition state (TS) are expected to be open-shell singlet states, while the product complex (PC) and products will be closed-shell singlet states. This is similar to the $\text{BrO} + \text{CH}_3\text{O}_2 \rightarrow \text{HOBr} + \text{CH}_2\text{O}_2$ reaction, which was studied by us recently (13). It was found in this work (13) that most density functionals and the MP2 method were unable to locate the open-shell singlet TS for the singlet reaction surface, with the exceptions of the M06-2X and BH&HLYP functionals (13). Our previous study (13) shows the inadequacy of most functionals used, and also the inadequacy of the underlying UHF wavefunction used in the MP2 calculations, in dealing with the open-shell singlet TS {see reference (13) for details}. In an earlier study of the $\text{BrO} + \text{CH}_3\text{O}_2$ reaction by Guha and Francisco, in which the QCISD method was employed, a TS for the singlet reaction channel could not be located, almost certainly also because of the inadequacy of the underlying HF wavefunction used (14). Summarizing, based on previous results (13,14), for this type of reaction, simple correlation methods based on UHF wavefunctions appear to be inadequate for dealing with open-shell singlet TSs, while the M06-2X functional seems to be a more appropriate choice.

The first computational study of the $\text{BrO} + \text{HO}_2$ reaction was carried out by Kaltsoyannis and Rowley (15). They investigated three reaction channels, formation of (i) $\text{HOBr} + \text{O}_2(X^3\Sigma^-_g)$, (ii) $\text{HOBr} + \text{O}_2(a^1\Delta_g)$, and (iii) $\text{HBr} + \text{O}_3$. They employed CCD/6-311G** calculations for geometry optimization and carried out fixed point CCSD(T)/6-311G** calculations at the energy minima and transition states obtained. They concluded that the channel with the largest rate coefficient is (i) as it had the smallest computed reaction barrier. The barriers and reaction enthalpies for these channels were computed as (i) -2.9, -52.6 kcal.mol⁻¹, (ii) 15.8, -37.3 kcal.mol⁻¹ and (iii) 8.1, -10.0 kcal.mol⁻¹. However, the results of this work must be treated with caution particularly with respect to the singlet pathways (ii) and (iii), as it appears that restricted wavefunctions have been used and hence only closed-shell singlet species on the singlet reaction surface were considered (15). No rate coefficients were calculated by Kaltsoyannis and Rowley (15) and hence a comparison cannot be made in their work with experimental rate coefficients. In related work, Guha and Francisco (16-18) have studied possible isomers of HBrO_3 , obtained from $\text{BrO} + \text{HO}_2$, investigating their structures, relative energies, vibrational spectra, as well as their isomerization and reaction pathways. In these calculations, geometry optimization was performed at the QCISD level with fixed point calculations carried out at the QCISD(T) level.

In this present work five reaction channels for $\text{BrO} + \text{HO}_2$ were investigated:-





Reaction (2) is potentially important as it produces ozone and reactions (3) and (4) were included because they both produce OH. They could be atmospherically significant if their rate coefficients are comparable or higher than the rate coefficients of reactions 1(a) and 1(b).

The aim is to use state-of-the-art wavefunction and DFT methods to investigate the reaction mechanism of the BrO + HO₂ reaction, and to determine, for each channel, the energies of the RC, TS, PC and products relative to the reactants. It was also proposed to compute reaction rate coefficients (k) for the channel with the largest values of k in the atmospherically relevant temperature range, 200-400 K, for comparison with available experimental values. This will be the first time that rate coefficients have been calculated for this reaction from potential surfaces derived from electronic structure calculations. It is expected that channels 1a and 1b will be the most important kinetically as, in a discharge-flow mass spectrometric study (8), HOBr has been observed as the main reaction product in the temperature range 300-441 K and no O₃ was detected (8). This allowed a limit to be placed on the rate coefficient ratio $k_2/k_{(1a+1b)}$ of less than 1.5×10^{-2} (8).

Computational Details

(a) Electronic structure calculations

As in our earlier studies of atmospherically important reactions (19-22), the overall strategy used for each reaction channel is to obtain the geometries and harmonic vibrational frequencies of the stationary points (reactants, RC, TS, PC, products) on the potential energy surface using DFT calculations with the M06-2X functional, as well as their energies relative to the reactants. The M06-2X functional was chosen because it has been shown to perform well for TS structures and reaction barrier heights in a number of benchmark studies (23-27). In addition, it has been found to perform well for open-shell singlet TSs for this type of reaction, as discussed above (13). For each TS, an IRC search is performed to ensure that the TS connects with the RC and the reactants, and the PC and the products. All M06-2X calculations were performed using GAUSSIAN09 (28) with the aug-cc-pVDZ basis sets for H, C and O and the aug-cc-pVDZ-PP basis set for Br (these are collectively denoted as AVDZ from now on). In addition to M06-2X calculations, some BD/AVDZ TS search and harmonic frequency calculations were also carried out (*vide infra*).

For the five reaction channels considered, (1a,1b, 2-4), three are triplet channels and two are singlet channels. For the triplet channels (1a), (3) and (4), triplet states were considered for the RC, the TS and the PC. For singlet channel (2), an open-shell singlet state (unrestricted-spin wavefunction with guess=mix; see GAUSSIAN online manual (28)) was considered for the RC, but geometry optimization led to a closed-shell intermediate (*vide infra*). Consequently, for this channel closed-shell singlet states were considered for the TS and the PC. For the singlet channel (1b), open-shell singlet states were considered for the RC and the TS. However, it was found that all of the

UHF based methods used in the present study give very poor computed relative electronic energies for $O_2(a^1\Delta_g)$ {with respect to $O_2(X^3\Sigma_g^-)$ }. The difficulty of obtaining reliable $O_2(a^1\Delta_g) - O_2(X^3\Sigma_g^-)$ separations in electronic structure calculations has been discussed elsewhere (29). Consequently, the $O_2(a^1\Delta_g)$ energy was estimated by adding the experimental $X^3\Sigma_g^- - a^1\Delta_g$ separation of O_2 {22.5 kcal.mol⁻¹ (30)} to the computed electronic energy of $O_2(X^3\Sigma_g^-)$ at each level of calculation used. The same was applied to the relative energy of the PC of this channel, assuming that the PCs of $O_2(a^1\Delta_g)$ and $O_2(X^3\Sigma_g^-)$ with HOBr have similar interactions and geometries.

The relative energies of stationary points obtained were then improved by fixed point calculations using high level *ab initio* methods. Initially, the RHF/UCCSD(T) method as implemented in MOLPRO (31) was used with the aug-cc-pVXZ (for H, C and O) and aug-cc-pVXZ-PP (for Br) basis sets, where X = T or Q. Extrapolation to the complete basis set (CBS) limit of computed relative electronic energies obtained with the AVQZ and AVTZ basis sets was carried out employing the $1/X^3$ formula. However, for the RC and the TS of channel 1(a), although the CCSD iterations in the UCCSD(T) calculations converged, the computed T_1 diagnostic values were rather large (~0.05 and ~0.1, respectively). In order to circumvent this problem, Brueckner theory was employed, as with Brueckner doubles (BD) the T_1 value is zero. BD(T)/AVQZ and BD(TQ)/AVTZ single energy calculations were carried out as implemented in GAUSSIAN09. Computed relative BD(T) energies obtained using the AVQZ and AVTZ basis sets were extrapolated to the CBS limit employing the $1/X^3$ formula (unless otherwise stated; *vide infra*). The highest level of relative electronic energies obtained in the present study is BD(TQ)/CBS, which combines the BD(T)/CBS value with the (Q) contribution from the {BD(TQ) – BD(T)} relative energies.

The ground electronic state of BrO is a $^2\Pi$ state, which is split into two spin-orbit components, $^2\Pi_{3/2}$ and $^2\Pi_{1/2}$, separated by 975.4 cm⁻¹ (32) with the $^2\Pi_{3/2}$ state lying lower. The $^2\Pi_{3/2}$ state lies lower than the position of the un-split $^2\Pi$ state by 487.7 cm⁻¹ (1.394 kcal.mol⁻¹). This value was used as a spin-orbit correction in the evaluation of all relative energies (*vide infra*), and the two spin-orbit BrO states were included in all rate coefficient calculations.

(b) Rate coefficient calculations

As will be discussed, of the five channels considered, 1(b) has a negative activation energy whereas 1(a), (2), (3) and (4) have positive activation energies (*vide infra*; see also Tables 1-5). Channel 1(b) was expected, therefore, to have the largest rate coefficients in the temperature range considered, 200-400K. Most rate coefficient calculations were made on this channel with some being carried out on channel 1(a). In order to give the correct orientations at the optimized stationary points for the subsequent rate coefficient calculations, the geometrical optimizations of the stationary points were re-done with the no-symmetry constraint ('nosym' keyword) in GAUSSIAN 09 (28). Cartesian coordinates were employed in all geometries for all *ab initio* and DFT calculations. The rate coefficients, which are high pressure limit values, were calculated using POLYRATE 2010-A (33) and VARIFLEX 1.0 (34).

For a reaction with a negative barrier there are in general two bottlenecks. The first bottleneck occurs on association of the two reactants, in which they need to overcome a centrifugal barrier, to form the RC. The second bottleneck is at the TS which separates the RC from the PC (35-37). Klippenstein and coworkers have introduced a two-transition state theory (38,39) which emphasized the importance of treating the two barriers at the energy (E) and angular momentum (J) resolved levels in order to obtain reliable rate coefficients for a reaction with a negative barrier. In the language of this two-transition state theory, the TS between the reactants and the RC is known as the outer transition state and the TS between the RC and the PC is known as the inner transition state. In general, both the outer transition state and the inner transition state will contribute to the overall reactive flux of the reaction. The overall rate coefficient (k_{overall}) for a reaction channel can be expressed in terms of the inner (k_{inner}) and outer (k_{outer}) rate coefficients associated with the inner and outer transition states as (38-43):-

$$1/k_{\text{overall}} = 1/k_{\text{inner}} + 1/k_{\text{outer}} \quad \text{----- (1)}$$

k_{overall} for a reaction channel was determined from

- (i) k_{outer} and k_{inner} calculated with VARIFLEX (34) (the k_{overall} value obtained is labelled $k_{\text{overall(i)}}$) and
- (ii) k_{outer} calculated with VARIFLEX and k_{inner} calculated with POLYRATE (33) (the k_{overall} value obtained is labeled $k_{\text{overall(ii)}}$).

For (i), k_{outer} values were evaluated using long-range transition state theory (TST) as used in phase-space-theory (PST). The long-range interaction potential used in these calculations was approximated by the potential $V(r) = -C_6/r^6$ where $C_6 = 1.5\alpha_1\alpha_2E_1E_2/(E_1+E_2)$ in which α_i are the isotropic polarizabilities and E_i are the ionization energies of the two reactants ($i=1,2$). For these calculations, the isotropic polarizability of the two reactants were computed at the M06-2X/AVDZ level and the ionization energies of BrO and HO₂ were taken from studies by u.v. photoelectron spectroscopy {10.46 eV for BrO (44) and 11.35 eV for HO₂ (45)}. For calculations of k_{inner} , energy and angular momentum resolved TST (E,J-TST) was used, with the BD(TQ)/CBS//M06-2X/AVDZ barrier height (corrected for spin-orbit splitting in BrO X²Π) (*vide infra*). The zero-point energy (ZPE) corrected barrier was used in VARIFLEX.

For (ii), k_{inner} values were calculated with POLYRATE (33) at different TST levels, namely, conventional transition state theory (TST), canonical variational transition state theory (CVT) and improved canonical variational transition state theory (ICVT), with different tunneling methods, including Wigner tunneling (W), zero-curvature tunneling (ZCT) and small-curvature tunneling (SCT) corrections. In TST calculations with POLYRATE, the classical electronic energy barrier was used with no ZPE correction.

For channel 1(b), the BD(TQ)/CBS//M06-2X/AVDZ minimum energy path (MEP) needed for POLYRATE was obtained by scaling the MEP curve at M06-2X/AVDZ level according to the equation utilised in our previous work (21).

Results and discussion

Ab initio/DFT results

The optimized structures of the stationary points of channels (1a), (1b), (2), (3) and (4) obtained in the present study are given in the Supplementary Material (Figures S1 to S7). Their relative electronic energies computed at various levels are listed in Tables 1, 2, 3, 4, and 5 respectively. Available heats of formation ($\Delta H_{f,298K}$) of the reactants and products, which were used to evaluate the reaction enthalpy ($\Delta H_{f,298K}^{RX}$) of each channel, are given in the Supplementary Material (Table S1). The reaction enthalpies of all five channels obtained in different ways are summarized in Table 6. The computed results for each channel obtained from the present work are discussed first, followed by a summary and comparison with results of other work.

Channel (1a): $\text{BrO} + \text{HO}_2 \rightarrow \text{HOBr} + \text{O}_2 (\tilde{X}^3\Sigma_g^-)$

The optimized M06-2X structures of the RC, TS and PC are shown in Figure S1, while the optimized structures of the TS obtained by the M06-2X and BD methods are compared in Figure S2. The TS of this channel located at the M06-2X/AVDZ level, had a small imaginary vibrational frequency of $162i \text{ cm}^{-1}$, which involves bending motions in both the BrO and HO₂ moieties. When UCCSD(T) calculations were used to improve the electronic energy of this TS obtained at the M06-2X/AVDZ geometry, a large T₁ value (~ 0.1) was obtained which suggested non-negligible multi-reference (MR) character. As mentioned above, in order to circumvent this problem, the BD method was employed. In this connection, BD/AVDZ geometry optimization and harmonic frequency calculations were performed on the TS to obtain its relative energy and geometry. A TS was located which had an imaginary frequency of $399i \text{ cm}^{-1}$ corresponding to the O-H stretching mode in the Br[O]--[H]O₂ unit. However, BD/AVDZ geometry optimization (and subsequent frequency) calculations were not carried out on the RC and PC, which are expected to have shallow minima, as their calculations would be very demanding computationally. Consequently, for the RC and PC, the best computed relative energies are at the CCSD(T)/CBS//M06-2X/AVDZ level, while for the TS, the best computed relative energy is at the BD(TQ)/CBS//BD/AVDZ level (see Table 1). Nevertheless, it is pleasing to see that for the relative reaction energy, ΔE^{RX} , the CCSD(T)/CBS and BD(TQ)/CBS values agree very well. This good agreement suggests that the CCSD(T)/CBS level should also perform well for the RC and PC.

There are significant differences in the optimized geometries of the TSs obtained at the two levels. The Br[O]--[H]O₂ bond in the M06-2X/AVDZ geometry is 1.77 Å, slightly shorter than the equivalent bond length in the RC of 1.87 Å, whereas in the BD/AVDZ TS it is 1.48 Å. Also, the

BD/AVDZ geometry has a dihedral angle ($\angle\text{Br-O-O-O}$) of 0.2° (the TS is virtually planar) whereas the M06-2X/AVDZ structure has a dihedral angle of 24.0° . Nevertheless, the difference between the computed $\Delta E(0\text{K})$ values obtained at the M06-2X/AVDZ and BD/AVDZ levels is small ($2.23 \text{ kcal.mol}^{-1}$; see Table 1). The energy of the TS relative to the reactants is negative at the BD/AVDZ level ($-1.78 \text{ kcal.mol}^{-1}$) but it is positive at the BD/AVTZ and BD/AVQZ levels (4.19 and $4.42 \text{ kcal.mol}^{-1}$ respectively). Because of the large change in relative energy on going from BD/AVDZ to BD/AVTZ, the AVDZ basis set is probably too small for a reliable TS relative energy. Much better agreement was obtained between the BD(T)/AVTZ//BD/AVDZ and BD(T)/AVQZ//BD/AVDZ relative energies (2.06 and $2.20 \text{ kcal.mol}^{-1}$). Regarding the computed relative reaction energy, $\Delta E^{(\text{RX})}$, it increases from the BD/AVDZ level to the BD/AVTZ level, but decreases from the BD/AVTZ level to the BD/AVQZ level (Table 1). Because the changes in the computed relative energies with the two sets of basis sets are in opposite directions, a CBS extrapolation technique seems inappropriate. Consequently, the average between the BD(T)/AVTZ and BD(T)/AVQZ values is taken as the CBS value. The closeness of the BD(T)/AVTZ and BD(T)/AVQZ values also suggests that these values are close to the result at basis set saturation. In addition, the computed BD(TQ)/CBS $\Delta E^{(\text{RX})}$ value obtained in this way agrees very well with the corresponding CCSD(T)/CBS value. Summarizing, this channel is exothermic with a recommended barrier height of $2.53 \text{ kcal.mol}^{-1}$ $\{\Delta E(0\text{K}) \text{ value}\}$ and reaction enthalpy ($\Delta H_{298\text{K}}^{\text{RX}}$) of $-47.5 \text{ kcal.mol}^{-1}$ $\{\text{BD(TQ)/CBS} + \text{SO(BrO)} \text{ values; see Table 1}\}$.

Channel (1b): $\text{BrO} + \text{HO}_2 \rightarrow \text{HOBr} + \text{O}_2$ ($\tilde{\text{a}}^1\Delta_g$)

The optimized M06-2X structures of the RC, TS and PC for this channel are shown in Figure S3, while the M06-2X/AVDZ and BD/AVDZ structures of the TS are compared in Figure S4. For the RC and TS, unrestricted wavefunctions were used together with guess=mix in order to obtain the open-shell singlet states, as mentioned above (for the TS structures, the computed spin density values at each atomic centre are given in Table S2). The distance between $\text{Br}[\text{O}]\dots[\text{H}]\text{O}_2$ in the RC was 1.87\AA and this decreased to 1.58\AA and 1.36\AA in the TSs optimized at the M06-2X/AVDZ (with imaginary frequency of $229i \text{ cm}^{-1}$) and BD/AVDZ (with imaginary frequency of $1391i \text{ cm}^{-1}$) levels respectively. The dihedral angle ($\angle\text{Br-O-O-O}$) of these TSs are 2.76° and 0.02° respectively. The computed $\Delta E(0\text{K})$ values of the TSs obtained by the M06-2X/AVDZ and BD/AVDZ methods differ by $0.05 \text{ kcal.mol}^{-1}$. The TS structures obtained by the two methods may be considered as qualitatively similar. In terms of the difference between the TSs for channels 1(b) and 1(a), the $\angle\text{Br-O-O-O}$ dihedral angle of 1(b) is smaller than that of 1(a) and the distance between $\text{Br}[\text{O}]\dots[\text{H}]\text{O}_2$ is smaller in 1(b) than 1(a).

Computed relative energies obtained at different levels of calculation are summarized in Table 2. For the TS, the BD/AVDZ calculations gave an open-shell singlet wavefunction as shown by the computed spin densities on the atomic centres. However, when the AVTZ and AVQZ basis sets were used in the BD(TQ)/AVTZ//BD/AVDZ and BD(T)/AVQZ//BD/AVDZ single energy calculations, the Brueckner wavefunctions converged to closed-shell singlet wavefunctions. These closed-shell singlet

states have significantly higher relative energies (see Table 2). Consequently, it was decided to use the M06-2X geometry of the TS for higher level BD calculations. With the M06-2X/AVDZ optimized TS geometry, the spin densities of the Brueckner wavefunctions computed with the AVTZ and AVQZ basis sets indicate open-shell singlet states (see Table S2).

In summary, this channel is exothermic with a recommended barrier height $\{\Delta E(0K)\}$ of -3.07 kcal.mol⁻¹ and reaction enthalpy (ΔH_{298K}^{RX}) of -25.0 kcal.mol⁻¹ {BD(TQ)/CBS +SO(BrO) values}.

Also, the multireference (MR) character of each of the TSs of channels 1(a) and 1(b) has been investigated by CASSCF and/or CASSCF/NEVPT2 calculations. The details of these MR calculations and their results are given in the Supplementary Material. The conclusion from these extra MR calculations is that the BD(TQ)/CBS results, summarised in Tables 1 and 2, are reliable.

Channel (2): BrO + HO₂ → HBr + O₃

For this channel, the optimized structures of the RC, TS and PC are shown in Figure S5. The RC is actually an intermediate, HOOOBr (labeled as IM2 in Figure 1). The barrier height, $\Delta E(0K)$, was computed as 10.93 kcal.mol⁻¹ at the BD(TQ)/CBS//M06-2X/AVDZ level (with BrO spin-orbit correction), significantly higher than the barrier heights of the reactions (1a) and (1b) respectively. The results obtained for this channel are similar to those obtained by Kaltsoyannis and Rowley (15). Both studies showed that BrO and HO₂ form a HOOOBr intermediate, which then proceeds to a TS to form the products. The M06-2X/AVDZ TS geometry obtained in the present work is very similar to that of the TS in ref.(15) (labeled ts5 in that work), which had been optimized at the CCD/6-311G** level. There was a slight difference in the geometry of this RC between our work and the work of ref.(15) in that the H and Br atoms in our RC are cis to each other (see Figure S5) whereas the H and Br atoms are trans to each other in the RC of ref.(15). The relative electronic energies of the RC, TS and separate products were calculated in ref.(15) as -17.21, 8.13 and -9.09 kcal.mol⁻¹ respectively at the CCSD(T)/6-311G**//CCD/6-311G** level, compared to the values obtained in this work of -19.57, 11.83 and -3.00 kcal.mol⁻¹ at the BD(TQ)/CBS//M06-2X/AVDZ level (with BrO spin-orbit correction). The significant difference between the computed reaction energies of the two studies (> 6 kcal.mol⁻¹) is probably due to the considerably smaller basis sets used by Kaltsoyannis and Rowley when compared with those used in the present study. In addition, although ozone is a closed-shell singlet, it has significant multireference (MR) character (46). In this connection, the BD(TQ) method is expected to perform better than the CCSD(T) method.

In summary, this channel is exothermic with a recommended barrier height $\{\Delta E(0K)\}$ of 10.93 kcal.mol⁻¹ and reaction enthalpy (ΔH_{298K}^{RX}) of -4.3 kcal.mol⁻¹ {BD(TQ)/CBS +SO(BrO) values}. The barrier is significantly higher than that of channels 1a and 1b, and therefore the rate coefficient of this channel will be significantly lower than those of 1a and 1b in the temperature range considered (200-400 K). This is consistent with the experimental result that HOBr has been observed as a major product of the BrO + HO₂ reaction. No O₃ has been detected experimentally from this reaction. Although small amounts of HBr have been observed, it was not possible to ascribe this to

channel (2) as it may arise from wall reactions or secondary reactions of HOBr (5,7,8).

For this channel, an equilibrium is assumed between the reactants and the intermediate, IM2, and as TS2 is high, at 10.93 kcal.mol⁻¹, this channel will not affect the overall rate coefficient (*vide infra*).

Channel (3): BrO + HO₂ → OBrO + OH

As far as we are aware, this is the first theoretical study of this channel, a reaction, which proceeds on a triplet potential energy surface. The optimized structure of the TS is shown in Figure S7. The reaction enthalpy { ΔH_{298K}^{RX} } computed at the BD(TQ)/CBS level is 14.9 kcal.mol⁻¹ (Tables 4 and 6) whereas that obtained at the M06-2X/AVDZ level is 29.9 kcal.mol⁻¹ (see Table 4). This large discrepancy in reaction enthalpy between the BD(TQ)/CBS and M06-2X/AVDZ methods probably arises from the inadequacy of the M06-2X method to account for the ground state of OBrO, which has MR character (47). Again, this shows the value of using BD theory in carrying out calculations on molecules, which have MR character. It is also pleasing that the ΔH_{298K}^{RX} value for this reaction calculated using available heats of formation (15.3 ± 2.8 kcal.mol⁻¹; see Tables 6 and S1) agrees very well with the BD(TQ)/CBS value reported in the present study. The computed barrier height { $\Delta E(0K)$ } for this reaction is very high (34.98 kcal.mol⁻¹, see Table 4). As a result, rate coefficients for this channel will be very much smaller than those of channels 1a,1b and 2 and are not expected to contribute to the overall reaction rate coefficient at temperatures of atmospheric importance.

In summary, this channel is endothermic with a recommended barrier height { $\Delta E(0K)$ } of 35.0 kcal.mol⁻¹ and reaction enthalpy (ΔH_{298K}^{RX}) of 14.9 kcal.mol⁻¹ {BD(TQ)/CBS + SO(BrO) values}.

Channel (4): BrO + HO₂ → BrOO + OH

As with channel (3), this is the first theoretical study of this channel. The results obtained are very similar to those obtained for channel (3) and channel (4) is not expected to contribute to the overall BrO + HO₂ rate coefficient at temperatures of atmospheric importance. The optimized structure of the TS is shown in Figure S6. The computed reaction enthalpy (ΔH_{298K}^{RX}) obtained at the BD(TQ)/CBS level (with BrO spin-orbit correction) is 5.9 kcal.mol⁻¹, in agreement with the reaction enthalpy calculated using available heats of formation (2.9 ± 3.5) kcal.mol⁻¹ (Table 6). However, the value calculated with the M06-2X/AVDZ functional is -4.9 kcal.mol⁻¹. The source of this difference is the M06-2X electronic energy of BrOO. As BrOO has some MR character (47), BD theory gives a more reliable electronic energy for BrOO than the M06-2X functional. The barrier height { $\Delta E(0K)$ } for this reaction is large, 37.8 kcal.mol⁻¹ calculated at the BD(T)/CBS level. In summary, this channel is endothermic with a recommended barrier height of 37.8 kcal.mol⁻¹ and reaction enthalpy (ΔH_{298K}^{RX}) of 5.9 kcal.mol⁻¹ {BD(TQ)/CBS + SO(BrO) values}.

Summary and comparison with other work

To provide reference values for our computed values, the reaction enthalpy ($\Delta H_{f,298K}^{RX}$) of each channel was calculated using available heats of formation ($\Delta H_{f,298K}$) of the reactants and products. The results (average literature values in Table 6) obtained are (1a) (-47.5 ± 2.1), (1b) (-25.0 ± 2.1), (2) (-7.1 ± 3.3), (4) (15.3 ± 2.8) and (3) (2.9 ± 3.5) kcal.mol⁻¹, which agree very well with the computed values of -47.5, -25.0, -4.3, 14.9 and 5.9 kcal.mol⁻¹ obtained at the BD(TQ)/CBS + SO(BrO) level from the present study (see Table 6). The reaction enthalpies ($\Delta H_{f,298K}^{RX}$) for reaction channels 1a, 1b and 2 computed by Kaltsoyannis and Rowley (15) with CCSD(T)/6-311G** calculations are in good agreement with the reference values for reactions 1a and 2, but their CCSD(T)/6-311G** value for reaction 1b is too negative by 12.3 kcal.mol⁻¹ compared to the reference value of (-25.0 ± 2.1) kcal.mol⁻¹. The recommended TS relative energies $\{\Delta E(0K)\}$ (including zero-point energy corrections) for these channels are (1a) 2.53, (1b) -3.07, (2) 10.93, (3) 35.0, (4) 37.81 kcal.mol⁻¹ (see Tables 1-5). Barrier heights computed in ref.(15) with CCSD(T)/6-311G** calculations for (1a), (1b) and (2) are -2.9, 15.8 and 8.1 kcal.mol⁻¹ respectively. It is notable that the barrier height of channel 1(a) in ref.(15) is negative whereas it is positive in the present work (the difference is 5.43 kcal.mol⁻¹). Overall, for channels (1a) and (2) the agreement of the barrier heights in ref.(15) with our values is moderate but for (1b) it is very poor (difference 18.9 kcal.mol⁻¹) probably for the reasons outlined in the Introduction.

Tables 3,4, 5 and 6

Rate coefficient results

(a) Schematic pathways for all channels and V_{MEP} , ΔZPE and Va^G curves for channel 1(b)

Figure 1 shows a schematic diagram of the five channels considered in this work, based on the computed relative energies obtained for the stationary points. As can be seen from this diagram, channel 1(a) is the most exothermic while 1(b) has the lowest barrier height. Channel 1(b), therefore, has the highest rate coefficients of the pathways considered and rate coefficients were calculated for this channel for temperatures in the range 200-400 K. The minimum energy path (MEP) computed at the BD(TQ)/CBS//M06-2X/AVDZ level (with BrO spin-orbit correction) was used for these calculations. 1(a) is the channel with the next lowest barrier height and some rate coefficient calculations were also carried out for this reaction using the MEP associated with the stationary points (best-estimate values) given in Table 1.

Figure 1

For channel 1(b), as described earlier, the higher level V_{MEP} curve was obtained from the lower level curve, at the M06-2X/AVDZ level, utilizing the scaling expression we have used previously (21), with relative energies obtained from fixed point calculations at the BD(TQ)/CBS level. The

V_{MEP} , ΔZPE and V_a^{G} curves obtained at the BD(TQ)/CBS//M06-2X/AVDZ level (with BrO spin-orbit correction) are shown in Figure 2. As can be seen, there is a dip in the ΔZPE curve near $s = +0.5 \text{ \AA}$. The change in the O-H stretching frequency contributes significantly to this change. At the M06-2X level, the O-H stretching frequency was computed as 3680 cm^{-1} in HO_2 , 2661 cm^{-1} in the TS and 3839 cm^{-1} in HOBr . The maximum of the V_a^{G} curve is not at $s = 0$, the maximum of the V_{MEP} curve, because of the ΔZPE contribution ($V_a^{\text{G}} = V_{\text{MEP}} + \Delta\text{ZPE}$). It occurs at $s = -0.509 \text{ \AA}$.

 Figure 2

(b) Computed rate coefficients

For channel 1(b), equation (1) was used to calculate $k_{\text{overall}(i)}$ from k_{inner} and k_{outer} using VARIFLEX (34). In these calculations, k_{outer} was calculated using PST and k_{inner} was calculated using energy (E) and angular momentum (J) resolved TST (E,J-TST). The results are shown in Figure S8. It was found that k_{outer} does not contribute significantly to the overall rate coefficient, $k_{\text{overall}(i)}$, even at low temperatures (see Figure S8 and Table S3). The major bottleneck is at the inner TS throughout the temperature range considered. The variational effect on k_{inner} was explored by evaluating this rate coefficient with variational transition state theory (VTST) using POLYRATE (33). k_{outer} was again evaluated using PST with VARIFLEX and $k_{\text{overall}(ii)}$ was evaluated using equation (1). Before this was done, however, values of k_{inner} computed at the E,J-TST level with VARIFLEX were checked against k_{inner} values computed with conventional TST with POLYRATE. The E,J-TST VARIFLEX values are slightly greater than the conventional TST POLYRATE values (see Figure S9 and Table S4). This was because the energy distribution in the reactants and TS are treated in a different way in E,J-TST compared to conventional TST, and the zero-point corrected barrier height ($-3.07 \text{ kcal.mol}^{-1}$) is used in the E,J-TST calculation whereas the classical electronic barrier height ($-3.05 \text{ kcal.mol}^{-1}$) is used in the conventional TST calculations (see footnote to Table S4). The results of k_{inner} obtained with POLYRATE at the TST, CVT and ICVT levels with different tunneling methods are shown in Figure 3 and Tables S5 and S6.

Since $k_{\text{ICVT/SCT}}$ is the highest level of variational transition state theory used in his work, these values were used in equation (1) for k_{inner} , with k_{outer} obtained from PST to obtain $k_{\text{overall}(ii)}$. The values used are given in Table S3 (for k_{outer}) and Table S6 (for k_{inner}), and the plots of k_{inner} , k_{outer} and $k_{\text{overall}(ii)}$ versus temperature are shown in Figure S10. Since the k_{inner} values are about two orders of magnitude smaller than the k_{outer} values, the inner TS is the major reaction bottleneck. Hence at a given temperature $k_{\text{overall}(ii)}$ is very close to k_{inner} and these two curves are virtually superimposed (see Figure S10).

Regarding the different variational transition state theory (VTST) calculations carried out in POLYRATE, as already indicated, the maxima of the V_{MEP} and V_a^{G} curves vs reaction coordinate, s , will in general not be the same. They will also in general be different from the maximum of the ΔG vs

s curve. The classical adiabatic ground state (CAG) correction, $\kappa^{\text{TST/CAG}}$, accounts for the fact that the conventional TS (at $s = 0$, the maximum of the V_{MEP} curve) is not at the maximum of the vibrationally adiabatic ground-state potential curve, $s^*(V_a^G)$ (48,49). A computed k at the TST (or CVT) level including a CAG and a multidimensional tunneling correction (MT; e.g. ZCT or SCT) can be related to k_{TST} (or k_{CVT}) via the equation:

$$k(\text{with tunnelling}) = \kappa^{\text{CAG}} \times \kappa(\text{tunneling}) \times k(\text{without tunnelling}),$$

$$\text{i.e. } k^{(\text{TST or CVT})/\text{MT}} = \kappa^{(\text{TST or CVT})/\text{CAG}} \times \kappa^{\text{MT}} \times k^{(\text{TST or CVT})}.$$

At the TST level, $\kappa^{\text{TST/CAG}} = \exp \{ \beta [V_a^G(s=0) - V_a^G(s^*)] \}$, where $\beta = 1/RT$. Generally, because $V_a^G(s^*) \geq V_a^G(s=0)$, $\kappa^{\text{TST/CAG}}$ is always ≤ 1 .

$\kappa^{\text{CVT/CAG}}$ is needed because the maximum of the ΔG curve and the V_a^G curves are not the same.

At the CVT level, $\kappa^{\text{CVT/CAG}} = \exp \{ \beta [V_a^G(s^{*\text{CVT(T)}}) - V_a^G(s^*)] \}$ (48,49).

Computed values of k , CAG and tunneling correction factors for channel 1(b) are listed in Table S8. This table shows that $(V_a^G(s=0) - V_a^G(s^*))$ is $-0.856 \text{ kcal.mol}^{-1}$, and the corresponding values of $\kappa^{\text{TST/CAG}}$ range from 0.112 at 200 K to 0.335 at 400 K. $(V_a^G(s^{*\text{CVT(T)}}) - V_a^G(s^*))$ is smaller in magnitude than $(V_a^G(s=0) - V_a^G(s^*))$ and, as a result, $\kappa^{\text{CVT/CAG}}$ values are closer to 1.00 than $\kappa^{\text{TST/CAG}}$, with values ranging from 0.974 at 200 K to 0.9114 at 400 K. For ICVT, since the generalized transition state (GTS) dividing surface is at $s^*(V_a^G)$, there is no CAG correction and $k^{\text{ICVT/MT}}$ can be related to k^{ICVT} as follows:-

$$k^{\text{ICVT/MT}} = \kappa^{\text{MT}} \times k^{\text{ICVT}}.$$

The computed rate coefficients at the same temperature show the expected trend of $k^{\text{TST}} \geq k^{\text{CVT}} \geq k^{\text{ICVT}}$ (see Figure 3 and Table S5) and the k^{CVT} values are almost identical to the k^{ICVT} values at temperatures in the region 200 K to 400 K. Since the computed tunneling factors (κ^{ZCT} and κ^{SCT}) are exactly 1.0 from 200 K to 400 K, the remaining correction factors are then the classical transmission coefficients ($\kappa^{\text{TST/CAG}}$ and $\kappa^{\text{CVT/CAG}}$). $\kappa^{\text{TST/CAG}}$ is ≈ 0.1 while $\kappa^{\text{CVT/CAG}}$ is ≈ 0.9 so $\kappa^{\text{TST/CAG}}$ leads to a large reduction of k^{TST} whereas $\kappa^{\text{CVT/CAG}}$ leads to a small reduction of k^{CVT} . The results obtained are shown in Figure 3 and Tables S5 and S6. The variational effect on the rate coefficients can be measured by the ratio $k^{\text{CVT}}/k^{\text{TST}}$. The closer this ratio is to unity, the smaller the variational effect. For channel 1(b), the $k^{\text{CVT}}/k^{\text{TST}}$ ratios are 0.127 and 0.352 at 200 K and 400 K respectively, indicating a significant variational effect. Figure 3 clearly shows that the computed rate coefficients occur in two groups. The larger set of rate coefficients consisting of k^{TST} and $k^{\text{TST/W}}$ and the lower set of consisting of the VTST rate coefficients (with and without tunneling corrections).

Figure 3

(c) Enthalpy of activation (ΔH^\ddagger) and entropy of activation (ΔS^\ddagger) contributions to the TST rate coefficient (k_{inner}) of channel 1(b).

All of the rate coefficients shown in Tables S5 and S6 of channel 1(b) (k_{inner} values calculated

with POLYRATE) show a negative temperature dependence (the values increase when the temperature decreases). This inverse temperature dependence is present in all the computed rate coefficients (e.g. TST, CVT, ICVT and CVT/SCT). In order to investigate this effect, the contributions of the activation entropy and enthalpy at different temperatures to the activation free energy are examined, and to simplify the discussion, only the corresponding rate coefficient values at the TST level are considered.

In TST, a bimolecular reaction rate coefficient can be written as:-

$$k = (k_B T / h c^0) \exp(-\Delta G^\ddagger / k_B T) = (k_B T / h) \exp(\Delta S^\ddagger / k_B) \exp(-\Delta H^\ddagger / k_B T) \quad \text{-----}(2)$$

where c^0 is the gas-phase concentration under standard-state conditions, ΔH^\ddagger is the standard-state enthalpy of activation and ΔS^\ddagger is the standard state entropy of activation. ΔG^\ddagger is the standard-state free energy of activation. For channel 1(b), ΔH^\ddagger and ΔS^\ddagger are negative in the temperature range considered (200-400 K). Taking the natural logarithm of the above equation gives:-

$$\ln k = \ln(k_B T / h c^0) + \Delta S^\ddagger / k_B - \Delta H^\ddagger / (k_B T) \quad \text{-----}(3)$$

The term $\ln(k_B T / h c^0)$ increases with temperature. Also, as can be seen from Table 7, $\Delta S^\ddagger / k_B$ decreases slightly with temperature whereas $-\Delta H^\ddagger / (k_B T)$ shows a more significant decrease. As a result, $\ln k$ decreases with temperature because the $-\Delta H^\ddagger / (k_B T)$ term dominates over the $\ln(k_B T / h c^0)$ term. In Figure 4, changes in the terms in equation (3) relative to their values at 400K are plotted against $1000/T$. As shown in Table 7, the main contributor to the magnitude of $-\Delta G^\ddagger / (k_B T)$ (and hence $\ln k$) is the entropy term $\Delta S^\ddagger / k_B$ (lowering ΔH^\ddagger by 1.0 kcal.mol⁻¹ gave only a small increase in k at 298 K, of < 2 %), but the main term which determines the temperature dependence of $\ln k$ is the enthalpy term $-\Delta H^\ddagger / (k_B T)$ (see Table 7). This is one of the main conclusions of the study of this radical-radical reaction. The behaviour shown in Figure 4, of a decrease of $\ln k$ with temperature and a $\ln k$ vs $1000/T$ plot with a positive slope, compares with that of a reaction which has a negative ΔS^\ddagger and a positive ΔH^\ddagger which determines the temperature dependence of k . This shows an increase of $\ln k$ with temperature and a $\ln k$ vs $1000/T$ curve with negative slope.

 Figure 4 and Table 7

(d) Effect of channel (2) $\text{BrO} + \text{HO}_2 \rightarrow \text{HBr} + \text{O}_3$

As noted earlier, channel (2) proceeds via low-lying intermediate IM2 (HOOOBr), at -19.57 kcal.mol⁻¹, before passing over a TS, TS2 at 10.93 kcal.mol⁻¹, to form the products HBr + O₃. Experimentally, the overall reaction rate coefficient is the same as that of channel 1 (BrO + HO₂ → HOBr + O₂) in the temperature and pressure ranges 200-400 K and 1-760 torr. Also no HBr has been detected and there is no experimental evidence for formation of IM2 via, for example, mass spectrometric studies (5,7,8,12). It is expected that at high pressure some IM2 will be stabilised and this would enhance the overall BrO + HO₂ rate coefficient. However, so far all available experimental rate coefficients show no pressure dependence, suggesting that the formation of IM2 is insignificant in the pressure range studied. It appears that pressures required to achieve this may be

higher than have so far been used experimentally, and the formation of IM2 is probably not relevant from the perspective of atmospheric chemistry. Nevertheless, it would be valuable to study the intermediate IM2 (HOOBr), for example by infrared matrix isolation spectroscopy experiments or spectroscopic studies of this intermediate formed in a molecular beam.

(e) Comparison of computed k_{overall} values with experimental rate coefficients

Atkinson et al (3) have reviewed the available experimentally determined rate coefficients for the BrO + HO₂ reaction. Disregarding the early studies of Cox and Sheppard (2) which have a very low value, the reported rate coefficients at 298 K cover a range of just over a factor of two. The recommended value at 298 K, $(2.4 \pm 0.8) \times 10^{-11} \text{ cm}^3 \text{ molecule}^{-1} \text{ s}^{-1}$, is the mean of the values from references (4-8,11,12). The experimental temperature dependence of k in reference (3) has been obtained by taking the mean of the values of references (5,7,8,12), but adjusting the pre-exponential factor in an Arrhenius fit to give the recommended value at 298 K. These recommended values (3) in the temperature range 210-360 K are shown in Table 8. To compare our computed rate coefficients with these experimentally derived values, the computed $k_{\text{overall(ii)}}$ values for channel 1(b) shown in Table S7 were used. As can be seen from this table, the $k_{\text{overall(ii)}}$ values are very close to the $k_{\text{ICVT/SCT}}$ (k_{inner}) values because the inner TS is the main reaction bottleneck. Comparison of the $k_{\text{overall(ii)}}$ values obtained in this way with available experimental values is shown in Figure 5, and with the recommended experimental values of Atkinson et al. (3) in Table 8 and Figure 6. As can be seen from Table 8, the computed $k_{\text{overall(ii)}}$ values are too low (by a factor of ~ 8 at 210 K) and by an order of magnitude at higher temperatures. Also, although the $k_{\text{overall(ii)}}$ values do show a negative temperature dependence, this is not as pronounced as the temperature dependence of the experimental values. The TST rate coefficients agree better with the experimental k values particularly in the lower temperature region (200-300 K) and show a greater temperature dependence. Although it is difficult to identify the reason for these differences in experimental and computed values, they probably originate from the low level MEP, geometry and frequencies, which in this case are obtained at the M06-2X/AVDZ level. Previous work from our group (50) has shown that calculated k values obtained with different low levels (MEP, geometries and frequencies) with the same high level barrier height can give k values with a spread of an order of magnitude. This indicates that the ZPE and entropy contributions from different low levels, which are used in the higher level calculations, are very important in determining the rate coefficient k . Inaccuracies in ΔH^\ddagger and the detailed shape of the higher level potential energy curve obtained at the BD(TQ)/CBS//M06-2X/AVDZ level (with BrO spin-orbit correction) used in the variational TST calculations also need to be considered.

Some VTST rate coefficient calculations were also made for channel 1(a) using the MEP derived from the relative energies of the stationary points (reactants, RC,TS,PC and products) obtained from the calculations described earlier (see Table 1 for best-estimate relative energies). The rate coefficients obtained for this channel in the temperature range 200-400 K are at least four orders

of magnitude lower than those for channel 1(b).

Table 8

This work has led to a greater understanding of the energetics and mechanism of the BrO + HO₂ reaction and shown that HOBr (X¹A') + O₂(a¹Δ_g), rather than HOBr (X¹A') + O₂(X³Σ_g⁻), is the dominant reaction pathway with the higher rate coefficient. A similar investigation is needed for the ClO + HO₂ reaction to see if HOCl (X¹A') + O₂(a¹Δ_g), rather than HOCl (X¹A') + O₂(X³Σ_g⁻), is the kinetically most important channel. However, the experimental rate coefficient of the ClO + HO₂ reaction, which also shows a negative temperature dependence, is lower than that of BrO + HO₂ in the temperature range 200-400 K by a factor of ~5 (3). Therefore ClO + HO₂ is probably less important than BrO + HO₂ in contributing to ozone depletion in the atmosphere.

Figures 5 and 6

Concluding remarks

The energetics and mechanism of the BrO + HO₂ reaction have been investigated by carrying out *ab initio*/DFT calculations. Of the five reaction channels considered, channel 1(a), HOBr (X¹A') + O₂(X³Σ_g⁻), is the most exothermic while channel 1(b), HOBr (X¹A') + O₂(a¹Δ_g), has the lowest activation energy and therefore the highest rate coefficient. This result contrasts with that obtained in ref.(15) where channel 1(a) was computed to be the most exothermic and to have the lowest activation energy. This arose because it appears that in ref.(15) restricted calculations were performed and the wavefunctions obtained for the TSs were closed-shell rather than open-shell singlets. In this present work unrestricted calculations were carried out and Brueckner theory was used. For channel 1(b), for the converged wavefunction for each TS, spin-densities on each centre were investigated to check that the wavefunction corresponds to an open-shell rather than a closed-shell singlet.

Rate coefficients were calculated for channels 1(a) and 1(b) for BrO + HO₂ for the first time. These calculations were performed on channel 1(b), HOBr (X¹A') + O₂(a¹Δ_g), with two-state transition state theory in which values of k_{inner} and k_{outer} are calculated and used to determine the overall rate coefficient (k_{overall}). The inner transition state was identified as the major bottleneck of the reaction with the outer transition state having very little effect on the overall rate coefficient in the temperature range considered, 200 – 400 K. Studying the entropy, enthalpy and free energy of activation as a function of temperature shows that the main contributor to the magnitude of -ΔG[#]/(k_BT) (and hence lnk) is the entropy term ΔS[#]/k_B, but the main term which determines the temperature dependence of lnk is the enthalpy term -ΔH[#]/(k_BT). Some rate coefficient calculations were also performed for channel 1(a) which show that it is much slower than channel 1(b) in the

temperature range considered. On comparing the computed rate coefficients (k_{overall}) with the experimental rate coefficients, the computed values at the highest level (k_{inner} at the ICVT/SCT level) show a negative temperature dependence as is observed experimentally but are approximately an order of magnitude lower than the experimental values. In studies by Klippenstein et al.(38,40,42) on some reactions with negative or small positive barriers, employing the two-state TS model, it has been found that both TSs contribute to the overall rate coefficient with the outer TS dominating at lower temperatures and the inner TS dominating at higher temperatures. Channel 1(b) of BrO + HO₂ is different in that the inner TS bottleneck controls the rate coefficient, k , at all temperatures studied. The value of k at any temperature is determined mainly by the entropy of activation, ΔS^\ddagger , whereas the temperature dependence of k is determined mainly by the enthalpy of activation, ΔH^\ddagger . In the dual-level approach used in this work to calculate rate coefficients for channels 1(a) and 1(b), while the higher level IRC/ V_{MEP} energies are at the BD(TQ)/CBS//M06-2X/AVDZ or CCSD(T)/CBS//M06-2X/AVDZ level (M06-2X/AVDZ curves scaled with higher level fixed point relative energies), ΔS^\ddagger is calculated from vibrational and rotational constants in the TS and the reactants evaluated at the lower level, M06-2X/AVDZ. Errors in these vibrational and rotational constants, and hence ΔS^\ddagger values, are thought to be the main source of the differences between the computed and experimental values of k .

The theoretical basis of the dual level approach used in computing rate coefficients (as utilized in POLYRATE) is, in a way, similar to the computational strategy commonly adopted in composite electronic structure methods (e.g. G1, G2, etc.) for relative energies or thermodynamic quantities, e.g. enthalpy, where relative energies are computed with a high level correlation method and a large basis set, while geometries and vibrational frequencies are computed with a relatively low level method and a smaller basis set. The relative energies of fixed points on the IRC/ V_{MEP} at the higher level of the dual level approach have been computed at a near state-of-the-art level in the present study, and are expected to be within the commonly accepted chemical accuracy of 1 kcal.mol⁻¹. Generally, systematic improvements for single geometry energies at their level of calculation can be carried out and the associated uncertainties can be estimated, based on stepwise improvements in the correlation methods and/or basis sets employed. However, for the lower level calculations on geometries and vibrational frequencies of a medium size molecular system (say, of more than five atoms), the choice of the levels of methods/basis sets that can be used are restricted by the availability of analytical first and second energy derivatives with the methods considered (see reference 50). In the present study, where the entropy of activation is found to be the major contributor to the magnitude of the free energy of activation, the importance of obtaining reliable geometries and vibrational frequencies is evident, but it is computationally difficult to carry out systematic improvements on these computed quantities, because of the above-mentioned restriction. Also, as mentioned above, our previous study has shown that, with the same higher level barrier height but different lower level geometries and vibrational frequencies, the computed k values can differ by one order of magnitude (50). For the reaction studied in reference (50), $\text{H} + \text{CF}_3\text{CHFCF}_3 \rightarrow \text{CF}_3\text{CFCF}_3 + \text{H}_2$, the best computed barrier

height is positive and the enthalpy of activation makes a major contribution to the value of the rate coefficient. However, for the $\text{BrO} + \text{HO}_2 \rightarrow \text{HOBr} (X^1A') + \text{O}_2(a^1\Delta_g)$ reaction studied here, the barrier is submerged and the entropy of activation term makes the dominant contribution to the value of the computed rate coefficient. In this connection, the discrepancies between the highest level computed rate coefficients obtained in the present study and the best experimental values of reference (3) are most likely due to the inadequacy in the low level geometries and vibrational frequencies. In addition, the unexpected result that the computed overall rate coefficient (k_{overall}) obtained with the two TS approach is dominated by k_{inner} instead of k_{outer} is also due to the dominance of the entropy of activation of the inner TS rather than the enthalpy of activation (although the barrier is negative, its effects are small when entropy of activation dominates). In this connection, it is also found that reducing the inner barrier height (by a few kcal.mol^{-1}) has negligible effects on the computed rate coefficients (k_{inner} and/or k_{overall}). This result should provide some warning when trying to match computed and experimental rate coefficients by varying the computed barrier height, as the differences between theoretical and experimental values could be due to the entropy of activation, not the barrier height. In conclusion, in calculating rate coefficients, the entropy of activation can be important, and in the present case, it has been shown to be more important than the barrier height or the enthalpy of activation. Specifically, for channel 1(b) $\text{BrO} + \text{HO}_2 \rightarrow \text{HOBr} (X^1A') + \text{O}_2(a^1\Delta_g)$, the entropy of activation determines the magnitude of computed rate coefficients, while the enthalpy of activation determines their temperature dependence.

Acknowledgments

The authors are grateful to the Research Grant Council (RGC) of the Hong Kong Special Administrative Region (HKSAR, Grant Numbers: PolyU 5011/12P, 5018/13P and 15013/15P), the Research Committee of the Hong Kong Polytechnic University (Account No. A-PK41 and G-YBAV) and NERC (UK) for support, and the National Service for Computational Chemistry Software (NSCCS), EPSRC (UK) for providing computational resources.

References

1. Y.L.Yung, J.P.Pinto, R.T.Watson and S.P.Sander Atmospheric Bromine and Ozone Perturbations in the Lower Stratosphere *J.Atmos Science* 37, 1980, 339-353
2. R.A.Cox and D.W.Sheppard Rate coefficient for the reaction $\text{BrO} + \text{HO}_2$ at 303 K *J.C.S.Faraday II*, 78, 1982, 1383-1389
3. R.Atkinson, D.L.Baulch, R.A.Cox, J.N.Crowley, J.N. Hampson et al. Evaluated kinetic and photochemical data for atmospheric chemistry Vol III Gas-phase reactions of inorganic halogens *Atmos Chem Phys* 7, 2007, 981-1191
4. W.J.Bloss, D.Rowley, R.A.Cox and R.L.Jones Rate coefficient for the $\text{BrO} + \text{HO}_2$ reaction at 298 K *PCCP* 4, 2002, 3639-3647
5. V.Bedjanian, V.Riffault and G.Poulet Kinetic study of the reactions of BrO radicals with HO_2 and DO_2 *J.Phys Chem A* 105, 2001, 3167-3175
6. J.M.Cronkite, R.E.Stickel, J.M.Nicovich and P.H.Wine Laser flash photolytic studies of radical-radical reaction kinetics: the $\text{BrO} + \text{HO}_2$ reaction *J.Phys Chem A* 102, 1998, 6651-6658
7. Z.Li, R.R.Fiedl and S.P.Sander Kinetics of the $\text{HO}_2 + \text{BrO}$ reaction over the temperature range 233-348 K *J.C.S. Faraday Trans* 93, 1997, 2683-2691
8. M.Larichev, F.Maguin, G.Le Bras and G.Poulet Kinetics and mechanism of the $\text{BrO} + \text{HO}_2$ reaction *J.Phys Chem* 99, 1995, 15911-15918
9. G.Poulet, M.Pirre, F.Maguin, R.Ramaroson and G.Le Bras Role of the $\text{BrO} + \text{HO}_2$ reaction in the stratospheric chemistry of bromine *Geophys Res Letts.* 19, 1992, 2305-2308
10. A.Mellouki, R.K.Talukdar and C.J.Howard Kinetics of the reactions of HBr with O_3 and HO_2 : the yield of HBr from $\text{HO}_2 + \text{BrO}$ *J.Geophys Research* 99, 1994, 22,949-22,954
11. I.Bridier, B.Veyret and R.Lesclaux Flash photolysis kinetic study of reactions of the BrO radical with BrO and HO_2 *Chem Phys Letts* 201, 1993, 563-568
12. M.J.Elrod, R.F.Meads, J.B.Lipson, J.V.Seeley and M.J.Molina Temperature dependence of the rate constant for the $\text{HO}_2 + \text{BrO}$ reaction *J.Phys Chem* 100, 1996, 5808-5812

13. D.E. Shallcross, K.E. Leather, A. Bacak, P. Xiao, E.P.F. Lee, M. Ng, D.K.W. Mok, J.M., Dyke, R. Hossaini, M.P. Chipperfield, M.A.H. Khan and C.J. Percival Reaction between CH_3O_2 and BrO radicals: a new source of upper troposphere lower stratosphere hydroxyl radicals J. Phys Chem A 119, 2015, 4618-4632
14. S. Guha and J.S. Francisco An *ab initio* study for the pathways for the reaction of CH_3O_2 and BrO radicals J. Chem Phys 118, 2003, 1779-1793
15. N. Kaltsoyannis and D.M. Rowley *Ab initio* investigations of the potential energy surfaces of the $\text{XO} + \text{HO}_2$ reaction (X= chlorine or bromine) PCCP 4, 2002, 419-427
16. S. Guha and J.S. Francisco Structures, vibrational spectra and relative energies of HBrO_3 isomers J. Phys Chem A 102, 1998, 2072-2079
17. S. Guha and J.S. Francisco An examination of the reaction pathways for the HOOBr and HOBrO complexes formed from the $\text{HO}_2 + \text{BrO}$ reaction J. Phys Chem A 103, 1999, 8000-8007
18. S. Guha and J.S. Francisco A theoretical examination of the isomerization pathways for HBrO_3 isomers J. Phys Chem A 104, 2000, 9321-9327
19. M. Ng, D.K.W. Mok, E.P.F. Lee and J.M. Dyke A theoretical study of the mechanism of the atmospherically relevant reaction of chlorine atoms with methyl nitrate, and calculation of the reaction rate coefficients at temperatures relevant to the troposphere PCCP 2015, 17, 7463-7476
20. M. Ng, D. K. W. Mok, E.P. F. Lee, and J. M. Dyke
A theoretical investigation of the atmospherically important reaction between chlorine atoms and formic acid: Determination of the reaction mechanism and calculation of the rate coefficient at different temperatures Molecular Physics 113, 2015, 1511-1533
21. R. Chow, M. Ng, D. K.W. Mok, E.P.F. Lee, and J.M. Dyke
Rate coefficients of the $\text{Cl} + \text{CH}_3\text{C}(\text{O})\text{OCH}_3 \rightarrow \text{HCl} + \text{CH}_3\text{C}(\text{O})\text{OCH}_2$ reaction at different temperatures calculated by transition state theory with *ab initio* and DFT reaction paths J. Physical Chemistry A 118, 2014, 2040-2055
22. M. Ng, D.K.W. Mok, J.M. Dyke and E.P.F. Lee Decomposition reactions of hexafluoropropylene oxide (HFPO): rate coefficients calculated at different temperatures using *ab initio* and DFT reaction paths J. Fluorine Chem 159, 2014, 29-37

23. L. Goerigk and S. Grimme A thorough benchmark of density functional methods for general main group thermochemistry, kinetics, and noncovalent interactions *PCCP* 13, 2011, 6670-6688.
24. J.J. Zheng, Y. Zhao, and D.G. Truhlar The DBH24/08 Database and Its Use to Assess Electronic Structure Model Chemistries for Chemical Reaction Barrier Heights *Journal of Chemical Theory and Computation* 5, 2009, 808-821.
25. Y. Zhao, and D.G. Truhlar Density functionals with broad applicability in chemistry *Accounts of Chemical Research* 41, 2008, 157-167.
26. X.F. Xu; I.M. Alecu and D.G. Truhlar How well can modern density functionals predict internuclear distances at transition states? *Journal of Chemical Theory and Computation* 7, 2011, 1667-1676.
27. M. Balaganesh and B. Rajakumar Rate Coefficients and Reaction Mechanism for the Reaction of OH Radicals with (E)-CF₃CH=CHF, (Z)-CF₃CH=CHF, (E)-CF₃CF=CHF, and (Z)-CF₃CF=CHF between 200 and 400 K: Hybrid Density Functional Theory and Canonical Variational Transition State Theory Calculations *J. Phys. Chem. A*, 116, 2012, 9832-9842
28. Frisch, M. J.; Trucks, G. W.; Schlegel, H. B.; Scuseria, G. E.; Robb, M. A.; Cheeseman, J. R.; Scalmani, G.; Barone, V.; Mennucci, B.; Petersson, G. A.; Nakatsuji, H.; Caricato, M.; Li, X.; Hratchian, H. P.; Izmaylov, A. F.; Bloino, J.; Zheng, G.; Sonnenberg, J. L.; Hada, M.; Ehara, M.; Toyota, K.; Fukuda, R.; Hasegawa, J.; Ishida, M.; Nakajima, T.; Honda, Y.; Kitao, O.; Nakai, H.; Vreven, T.; Montgomery, J., J. A.; Peralta, J. E.; Ogliaro, F.; Bearpark, M.; Heyd, J. J.; Brothers, E.; Kudin, K. N.; Staroverov, V. N.; Keith, T.; Kobayashi, R.; Normand, J.; Raghavachari, K.; Rendell, A.; Burant, J. C.; Iyengar, S. S.; Tomasi, J.; Cossi, M.; Rega, N.; Millam, J. M.; Klene, M.; Knox, J. E.; Cross, J. B.; Bakken, V.; Adamo, C.; Jaramillo, J.; Gomperts, R.; Stratmann, R. E.; Yazyev, O.; Austin, A. J.; Cammi, R.; Pomelli, C.; Ochterski, J. W.; Martin, R. L.; Morokuma, K.; Zakrzewski, V. G.; Voth, G. A.; Salvador, P.; Dannenberg, J. J.; Dapprich, S.; Daniels, A. D.; Farkas, Ö.; Foresman, J. B.; Ortiz, J. V.; Cioslowski, J.; Fox, D. J. *Gaussian 09; Revision B.01 ed.*; Gaussian, Inc.: Wallingford CT, 2010.
29. E. Drougas, and A.M. Kosmas Computational studies of (HIO₃) isomers and the HO₂ + IO reaction pathways *J. Phys. Chem. A* 109. 2005, 3887-3892.
30. K.P. Huber and G. Herzberg *Molecular Spectra and Molecular Structure IV Constants of Diatomic Molecules*

van Nostrand New York 1979

31. H.-J. Werner, P. J. Knowles, G. Knizia, F. R. Manby, M. Schütz, P. Celani, T. Korona, R. Lindh, A. Mitrushenkov, G. Rauhut, K. R. Shamasundar, T. B. Adler, R. D. Amos, A. Bernhardsson, A. Berning, D. L. Cooper, M. J. O. Deegan, A. J. Dobbyn, F. Eckert, E. Goll, C. Hampel, A. Hesselmann, G. Hetzer, T. Hrenar, G. Jansen, C. Köppl, Y. Liu, A. W. Lloyd, R. A. Mata, A. J. May, S. J. McNicholas, W. Meyer, M. E. Mura, A. Nicklass, D. P. O'Neill, P. Palmieri, D. Peng, K. Pflüger, R. Pitzer, M. Reiher, T. Shiozaki, H. Stoll, A. J. Stone, R. Tarroni, T. Thorsteinsson, and M. Wang, MOLPRO, version 2012.1, a package of ab initio programs, see <http://www.molpro.net>.

32. B.J.Drouin, C.E.Miller, H.S.P.Muller, and E.A. Cohen. The rotational spectra, isotopically independent parameters, and interatomic potentials for the X-1 (2)Pi(3/2) and X-2 (2)Pi(1/2) states of BrO J. Mol.Spectrosc. 205, 2001, 128-138.

33. J.Zheng, S.Zhang, B.J. Lynch, J.C. Corchado, Y.Y.Chuang; P.L.Fast; W.P.Hu; Y.P.Liu; G.C.Lynch, K.A.Nguyen *et al.* POLYRATE version 2010-A (June, 2010), Copyright 1988-2010 D. G. Truhlar and Regents of the University of Minnesota, Minneapolis, Minnesota, U.S.A.

34. S.J.Klippenstein, A.F.Wagner, S.H.Robertson, R. Dunbar, and D.M. Wardlaw Variflex software, Version 1.0, <http://chemistry.anl.gov/variflex>

35. W.H.Miller Unified statistical model for "complex" and "direct" reaction mechanisms J.Chem Phys 65, 1976, 2216-2223

36. J.C. Light Phase-Space Theory of Chemical Kinetics J. Chem. Phys. 40, 1964, 3221-3229

37. B.C.Garrett and D.G. Truhlar Canonical unified statistical model. Classical mechanical theory and applications to collinear reactions J. Chem. Phys. 76, 1982, 1853-1858.

38. E.E.Greenwald, S.W.North, Y. Georgievskii, and S.J. Klippenstein A two transition state model for radical-molecule reactions. Case study of the addition of OH to C₂H₄ J. Phys. Chem. A 109, 2005, 6031-6044.

39. Y.Georgievskii and S.J. Klippenstein Long-range transition state theory J. Chem. Phys. 122, 2005, 194103.

40. E.E.Greenwald, S.W.North, Y.Georgievskii and S.J.Klippenstein A two transition state model

for radical-molecule reactions. Applications to isomeric branching in the OH-isoprene reaction
J.Phys Chem A 111, 2007, 5582-5592

41. W.C.Tsai and W.P.Hu Theoretical analysis on the kinetic isotope effects of bimolecular nucleophilic substitution (S_N2) reactions and their temperature dependence
Molecules 18, 2013, 4816-4843

42. P.Zhang, S.J.Klippenstein and C.K.Law *Ab initio* kinetics for the decomposition of hydroxybutyl and butoxy radicals of n-butanol J.Phys Chem A 117, 2013, 1890-1906

43. W.P.Hu and D.G.Truhlar Factors affecting competitive ion-molecule reactions: $ClO^- + C_2H_5Cl$ and C_2D_5Cl via E2 and S_N2 channels JACS 118, 1996, 860-869

44. J.M. Dyke, S.D. Gamblin, N. Hooper, E.P.F. Lee, A. Morris, D.K.W. Mok and F.T. Chau.
A study of the BrO and BrO₂ radicals with vacuum ultraviolet photoelectron spectroscopy
J. Chem. Phys., 112, 2000, 6262-6274

45. J.M. Dyke, N.B.H. Jonathan, A. Morris, and M.J. Winter Vacuum ultraviolet photoelectron spectroscopy of transient species 13. Observation of the X^3A'' state of HO₂⁺
Molecular Physics 44, 1981, 1059-1066.

46. W.D. Laidig and H.F. Schaefer Large multi-configuration self-consistent-field wave functions for the ozone molecule J. Chem. Phys. 74, 1981, 3411-3414

47. L.F. Pacios and P.C. Gomez Bonding in bromine oxides: Isomers of BrO₂, Br₂O₂ and BrO₃
J. Mol. Struct. A 467, 1999, 223-231.

48. A. Fernández-Ramos, J.A. Miller, S. Klippenstein, and D.G. Truhlar
Modelling the kinetics of bimolecular reactions Chem. Rev. 106, 2006, 4518-4584.

49. A. Fernandez-Ramos, B.A. Ellingson, B.C. Garret, and D.G. Truhlar Variational transition state theory with multidimensional tunneling
in Reviews in Computational Chemistry Vol. 23; Chapter 3 pp. 125-232, 2007
Lipkowitz, K. B.; Cundari, T. R. (Eds.) Wiley-VCH: Hoboken, NJ.

50. M. Ng, D.K.W. Mok, E. P.F. Lee, and J. M. Dyke
Rate coefficients of the $CF_3CHF_3 + H \rightarrow CF_3CF_3 + H_2$ reaction at different temperatures calculated by transition state theory with *ab initio* and DFT reaction paths

J.Computational Chemistry 34, 2013, 545-557

51.S.P.Sander, J. Abbatt, J. R. Barker, J. B. Burkholder, R. R. Friedl, D. M. Golden, R. E. Huie, C. E. Kolb, M. J. Kurylo, G. K. Moortgat, V. L. Orkin and P. H. Wine Chemical Kinetics and Photochemical Data for Use in Atmospheric Studies, Evaluation No. 17," JPL Publication 10-6, Jet Propulsion Laboratory, California Institute of Technology, Pasadena, June 10th, 2011.

<http://jpldataeval.jpl.nasa.gov/pdf/JPL%2010-6%20Final%2015June2011.pdf>

TABLES

Table 1. Computed relative energies (kcal.mol⁻¹) of the reactant complex (RC), transition state (TS) ($\Delta E(0K)$ for relative energy of TS with zero-point correction), product complex (PC), separate products (ΔE^{RX}), and reaction enthalpy at 298 K (ΔH_{298K}^{RX}) with respect to the separate reactants, of channel 1(a) $BrO + HO_2 \rightarrow HOBr + O_2 (X^3\Sigma_g^-)$ obtained at different levels (all values in the table have been corrected for a spin-orbit correction in BrO)^a.

All relative energies are obtained at the CCSD(T)/CBS//M06-2X/AVDZ level apart from the relative energy of the TS which is obtained at the BD(TQ)/CBS//BD/aVDZ level (see text).

Level	RC	TS	$\Delta E(0K)$	PC	ΔE^{RX}	ΔH_{298K}^{RX}
M06-2X/AVDZ	-5.07	-5.06	-4.01 ^b	-52.26	-50.89	-50.4 ^d
BD/AVDZ		-1.74	-1.78 ^c		-49.62	-49.1 ^e
BD/AVTZ		4.24	4.19 ^c		-48.24	-47.8 ^e
BD/AVQZ		4.47	4.42 ^c		-48.54	-48.1 ^e
BD(T)/AVTZ//BD/AVDZ		2.11	2.06 ^c		-47.82	-47.3 ^e
BD(T)/AVQZ//BD/AVDZ		2.25	2.20 ^c		-47.99	-47.5 ^e
BD(T)/CBS//BD/AVDZ		2.35 ^f	2.30 ^{c,f}		-47.91 ^g	-47.4 ^e
BD(TQ)/AVTZ//BD/AVDZ		2.35	2.30 ^c		-47.19	-46.7 ^e
(Q) contribution ^h		0.22			-0.050	
Composite BD(TQ)/CBS ⁱ //BD/AVDZ		2.58	2.53 ^c		-47.96	-47.5 ^e
CCSD(T)/AVTZ//M06-2X/AVDZ	-4.02			-48.96	-47.38	-46.9 ^d
CCSD(T)/AVQZ//M06-2X/AVDZ	-3.83			-49.33	-47.86	-47.3 ^d
CCSD(T)/CBS//M06-2X/AVDZ (1/X ³ :AVTZ/AVQZ) ^j	-3.68			-49.62	-48.20	-47.7 ^d
Best estimates	-3.68	2.58	2.53 ^c	-49.62	-47.96 -47.46 ^k	-47.5 ^e

^a For BrO, the ground electronic state is $\tilde{X}^2\Pi$, and the experimental equilibrium spin-orbit (SO) separation between the $\tilde{X}^2\Pi_{1/2}$ and $\tilde{X}^2\Pi_{3/2}$ states is 975.43 cm⁻¹ (or 2.7889 kcal.mol⁻¹) (ref.32). Using this SO splitting, the $\tilde{X}^2\Pi_{3/2}$ SO state of BrO is lower than the unperturbed $\tilde{X}^2\Pi$ state by 1.39 kcal.mol⁻¹.

^b The zero-point energy corrections were computed at M06-2X/AVDZ level.

^c The zero-point energy corrections were computed at BD/AVDZ level.

^d Using $\Delta ZPE + \Delta E_{298K}^{vib}$ from M06-2X frequency calculations (=0.505 kcal.mol⁻¹)

^e Using $\Delta ZPE + \Delta E_{298K}^{vib}$ from BD frequency calculations (=0.474 kcal.mol⁻¹)

^f The BD(T)/CBS value was obtained by using the 1/X³ formula with the reaction energy at BD(T)/AVTZ and BD(T)/AVQZ levels respectively.

^g The BD(T)/CBS value was taken as the average of the relative energy at BD(T)/AVTZ and BD(T)/AVQZ levels respectively (see text).

^h The (Q) contribution was calculated as: $BD(TQ)/AVTZ - BD(T)/AVTZ$

ⁱ Assuming additivity in a composite approach: $BD(TQ)/CBS = BD(T)/CBS + (Q)$

^j The CCSD(T)/CBS value was obtained by using the $1/X^3$ formula with the reaction energy at CCSD(T)/AVTZ and CCSD(T)/AVQZ levels respectively.

^k Zero-point corrected value computed by using frequencies obtained at BD/AVDZ level

Table 2. Computed relative energies (kcal.mol⁻¹) of the reactant complex (RC), transition state (TS) ($\Delta E(0K)$ for relative energy of TS with zero-point correction), separate products (ΔE^{RX}), and reaction enthalpy at 298 K (ΔH_{298K}^{RX}) with respect to the separate reactants, of channel 1(b) $\text{BrO} + \text{HO}_2 \rightarrow \text{HOBr} + \text{O}_2$ ($\tilde{a}^1\Delta_g$) obtained at different levels, used in the calculations of rate coefficients (all values in the table have been corrected for a spin-orbit correction in BrO)^a.

All relative energies are obtained at the CCSD(T)/CBS//M06-2X/AVDZ level apart from the relative energy of the TS which is obtained at the composite BD(TQ)/CBS level (see text).

Level	RC	TS ^b	$\Delta E(0K)^{c,d}$	ΔE^{RX} ^a	ΔH_{298K}^{RX}
M06-2X/AVDZ	-5.07	-3.50	-3.47	-36.81	-36.3 ^e
BD/AVDZ		-3.50 ; (2.05)	-3.52 ; (0.97)	-26.97 ^f	-26.6 ^{f,g}
BD/AVTZ		-0.49; (15.58)	-0.51 ; (14.50)	-25.81 ^h	-25.3 ^{e,h}
BD/AVQZ		-0.44; (15.86)	-0.46 ; (14.78)	-26.11 ^h	-25.6 ^{e,h}
BD(T)/AVTZ	-4.35	-3.32; (2.93)	-3.34 ; (1.85)	-25.18 ^h	-24.7 ^{e,h}
BD(T)/AVQZ	-4.25	-3.38; (3.10)	-3.40 ; (2.02)	-25.31 ^h	-24.8 ^{e,h}
BD(T)/CBS (1/X ³ :AVTZ/AVQZ)	-4.18	-3.42; (3.23)	-3.44 ; (2.15)	-25.48 ^h	-25.0 ^{e,h}
BD(TQ)/AVTZ	-4.20	-2.95; (4.21)	-2.97 ; (3.13)	-25.23 ^h	-24.7 ^{e,h}
(Q) contribution ⁱ	0.15	0.37; (1.28)		-0.050 ^h	
Composite BD(TQ)/CBS ^j	-4.03	-3.05; (4.52)	-3.07; (3.43)	-25.53 ^h	-25.0 ^{e,h}
CCSD(T)/AVTZ//M06 -2X/AVDZ				-24.75	-24.2 ^e
CCSD(T)/AVQZ//M06 -2X/AVDZ				-25.22	-24.7 ^e
CCSD(T)/CBS//M06-2 X/AVDZ (1/X ³ :AVTZ/AVQZ)				-25.50	-25.0 ^e
Best estimates	-4.03	-3.05; (4.52)	-3.07 ; (3.43)	-25.53 -25.03 ^k	-25.0 ^{e,h}

^a For BrO, the ground electronic state is $\tilde{X}^2\Pi$, and the experimental equilibrium spin-orbit (SO) separation between the $\tilde{X}^2\Pi_{1/2}$ and $\tilde{X}^2\Pi_{3/2}$ states is 975.43 cm⁻¹ (or 2.7889 kcal.mol⁻¹) (ref.32). Using this SO splitting, the $\tilde{X}^2\Pi_{3/2}$ SO state of BrO is lower than the unperturbed $\tilde{X}^2\Pi$ state by 1.39 kcal.mol⁻¹.

^b The first value was computed with M06-2X/AVDZ geometries, while the second value was computed with BD/AVDZ geometries. Note that at BD/AVDZ geometries, the computed spin densities with the AVTZ and AVQZ basis sets suggest that they are closed-shell singlet states, resulting in unreliable relative energies. (see Table S2).

^c The ZPE in the $\Delta E(0K)$ calculation of the first value was computed with the M06-2X/AVDZ geometry whereas the ZPE in the $\Delta E(0K)$ calculation of the value in brackets was computed with the BD/AVDZ geometry.

^d Using computed O_2 ($\tilde{X}^3\Sigma_g^-$) energies and the $\tilde{X}^3\Sigma_g^- - \tilde{a}^1\Delta_g$ separation of 7918.1 cm^{-1} ($=22.639 \text{ kcal.mol}^{-1}$) from spectroscopic T_e (ref.30).

^e Using $\Delta ZPE + \Delta E_{298K}^{vib}$ from M06-2X frequency calculations ($=0.505 \text{ kcal.mol}^{-1}$)

^f Electronic energies computed with optimized geometries at BD/AVDZ level

^g Using $\Delta ZPE + \Delta E_{298K}^{vib}$ from BD frequency calculations ($=0.372 \text{ kcal.mol}^{-1}$)

^h Electronic energies computed with optimized geometries at M06-2X/AVDZ level

ⁱ The (Q) contribution was calculated as: $BD(TQ)/AVTZ - BD(T)/AVTZ$

^j Assuming additivity in a composite approach: $BD(TQ)/CBS = BD(T)/CBS + (Q)$

^k Zero-point corrected value computed by using frequencies obtained at M06-2X/AVDZ level

Table 3. Computed relative energies (kcal.mol⁻¹) of the intermediate, transition state (TS) ($\Delta E(0K)$ for relative energy of TS with zero-point correction), separate products (ΔE^{RX}), and reaction enthalpy at 298 K (ΔH_{298K}^{RX}) with respect to the separate reactants, of channel (2) $BrO + HO_2 \rightarrow HBr + O_3$ obtained at different levels (all values in the table have been corrected for a spin-orbit correction in BrO)^a.

Level	Intermediate	TS	$\Delta E(0K)^b$	ΔE^{RX}	$\Delta H_{298K}^{RX c}$
M06-2X/AVDZ	-20.81	16.55	15.65	7.09	5.8
BD(T)/AVTZ//M06-2X/AVDZ	-19.57	12.36	11.47	-3.35	-4.7
BD(T)/AVQZ//M06-2X/AVDZ	-20.01	11.17	10.27	-3.71	-5.0
BD(T)/CBS//M06-2X/AVDZ (1/X ³ :AVTZ/AVQZ)	-18.94	10.30	9.40	-3.97	-5.3
BD(TQ)/AVTZ//M06-2X/AVDZ	-18.81	13.89	12.99	-2.38	-3.7
(Q) contribution ^d	0.76	1.52		0.97	
Composite BD(TQ)/CBS ^e //M06-2X/AVDZ	-19.57	11.83	10.93	-3.00	-4.3
Best estimates	-19.57	11.83	10.93	-3.00 -4.32 ^f	-4.3

^a For BrO, the ground electronic state is $\tilde{X}^2\Pi$, and the experimental equilibrium spin-orbit (SO) separation between the $\tilde{X}^2\Pi_{1/2}$ and $\tilde{X}^2\Pi_{3/2}$ states is 975.43 cm⁻¹ (or 2.7889 kcal.mol⁻¹) (ref.32). Using this SO splitting, the $\tilde{X}^2\Pi_{3/2}$ SO state of BrO is lower than the unperturbed $\tilde{X}^2\Pi$ state by 1.39 kcal.mol⁻¹

^b The zero-point energy corrections are computed at M06-2X/AVDZ level.

^c Using $\Delta ZPE + \Delta E_{298K}^{vib}$ from M06-2X frequency calculations (= -1.33 kcal.mol⁻¹).

^d The (Q) contribution was calculated as: BD(TQ)/AVTZ – BD(T)/AVTZ

^e Assuming additivity in a composite approach: BD(TQ)/CBS = BD(T)/CBS + (Q)

^f Zero-point corrected value computed by using frequencies obtained at M06-2X/AVDZ level

Table 4. Computed relative energies (kcal.mol⁻¹) of the transition state (TS) ($\Delta E(0K)$ for relative energy of TS with zero-point correction), separate products (ΔE^{RX}), and reaction enthalpy at 298 K (ΔH_{298K}^{RX}) with respect to the separate reactants, of channel (3) $BrO + HO_2 \rightarrow OBrO + OH$ obtained at different levels (all values in the table have been corrected for a spin-orbit correction in BrO)^a.

Level	TS	$\Delta E(0K)^b$	ΔE^{RX}	$\Delta H_{298K}^{RX c}$
M06-2X/AVDZ	49.63	49.01	31.50	29.9
BD(T)/AVTZ//M06-2X/AVDZ	33.35	32.73	15.55	13.9
BD(T)/AVQZ//M06-2X/AVDZ	33.58	32.96	14.92	13.3
BD(T)/CBS//M06-2X/AVDZ (1/X ³ :AVTZ/AVQZ)	33.75	33.13	14.47	12.9
BD(TQ)/AVTZ//M06-2X/AVDZ	35.20	34.58	17.59	16.0
(Q) contribution ^d	1.85		2.04	
BD(TQ)/CBS ^e //M06-2X/AVDZ	35.60	34.98	16.51	14.9
Best estimates	35.60	34.98	16.51, 14.65 ^f	14.9

^a For BrO, the ground electronic state is $\tilde{X}^2\Pi$, and the experimental equilibrium spin-orbit (SO) separation between the $\tilde{X}^2\Pi_{1/2}$ and $\tilde{X}^2\Pi_{3/2}$ states is 975.43 cm⁻¹ (or 2.7889 kcal.mol⁻¹) (ref.32). Using this SO splitting, the $\tilde{X}^2\Pi_{3/2}$ SO state of BrO is lower than the unperturbed $\tilde{X}^2\Pi$ state by 1.39 kcal.mol⁻¹. (this correction has been made to all values this table).

^b The zero-point corrections were computed at M06-2X/AVDZ level.

^c Using $\Delta ZPE + \Delta E_{298K}^{vib}$ from M06-2X frequency calculations (= -1.614 kcal.mol⁻¹).

^d The (Q) contribution was calculated as: BD(TQ)/AVTZ – BD(T)/AVTZ

^e Assuming additivity in a composite approach: BD(TQ)/CBS = BD(T)/CBS + (Q)

^f Zero-point corrected value computed by using frequencies obtained at M06-2X/AVDZ level.

Table 5. Computed relative energies (kcal.mol⁻¹) of the transition state (TS) ($\Delta E(0K)$ for relative energy of TS with zero-point correction), separate products (ΔE^{RX}), and reaction enthalpy at 298 K (ΔH_{298K}^{RX}) with respect to the separate reactants, of channel (4) $BrO + HO_2 \rightarrow BrOO + OH$ (all values in the table have been corrected for a spin-orbit correction in BrO)^a.

Level	TS	$\Delta E(0K)^b$	ΔE^{RX}	$\Delta H_{298K}^{RX, c}$
M06-2X/AVDZ	42.05	42.44	-3.69	-4.9
BD(T)/AVTZ//M06-2X/AVDZ	34.63	35.02	4.98	3.8
BD(T)/AVQZ//M06-2X/AVDZ	35.59	35.99	6.40	5.2
BD(T)/CBS//M06-2X/AVDZ	36.29	36.69	7.44	6.3
BD(TQ)/AVTZ//M06-2X/AVDZ	35.75	36.15	6.04	4.9
(Q) contribution ^d	1.12		-0.33	
BD(TQ)/CBS ^e //M06-2X/AVDZ	37.41	37.81	7.11	5.9
Best estimates	37.41	37.81	7.11, 5.12 ^f	5.9

^a For BrO, the ground electronic state is $\tilde{X}^2\Pi$, and the experimental equilibrium spin-orbit (SO) separation between the $\tilde{X}^2\Pi_{1/2}$ and $\tilde{X}^2\Pi_{3/2}$ states is 975.43 cm⁻¹ (or 2.7889 kcal.mol⁻¹) (ref.32). Using this SO splitting, the $\tilde{X}^2\Pi_{3/2}$ SO state of BrO is lower than the unperturbed $\tilde{X}^2\Pi$ state by 1.39 kcal.mol⁻¹.

^b The zero-point corrections were computed at M06-2X/AVDZ level.

^c Using $\Delta ZPE + \Delta E_{298K}^{vib}$ from M06-2X frequency calculations (= -1.185 kcal.mol⁻¹).

^d The (Q) contribution was calculated as: BD(TQ)/AVTZ – BD(T)/AVTZ

^e Assuming additivity in a composite approach: BD(TQ)/CBS = BD(T)/CBS + (Q)

^f Zero-point corrected value computed by using frequencies obtained at M06-2X/AVDZ level.

Table 6. Computed reaction enthalpies at the highest level in this work (BD(TQ)/CBS + SO(BrO)), the work of Kaltsoyannis and Rowley (15) at CCSD(T)/6-311G** and literature values at various levels of theory (c.f. Table S1 in the Supplementary Material) and experimental reaction enthalpies in kcal.mol⁻¹ of the five channels of the BrO + HO₂ reaction (1a,1b,2,3,4)

Channel	Level	ΔH_{298K}	Reference
1(a) BrO + HO ₂ → HOBr + O ₂ (³ Σ _g ⁻)	Experimental	-45.1	8
	BD(TQ)/CBS + SO(BrO) ^a	-47.5	This work
	CCSD(T)/CBS + SO(BrO) ^a	-47.7	This work
	CCSD(T)/6-311G** + SO(BrO) ^a	-51.4	15
	Best theoretical value from literature	-47.7±1.1	See supplementary materials
	Average literature values	-47.5±2.1	See supplementary materials
1(b) BrO + HO ₂ → HOBr + O ₂ ($\tilde{a}^1\Delta_g$)	Experimental	-25.0±2.1	8,51
	BD(TQ)/CBS + SO(BrO) ^a	-25.0	This work
	CCSD(T)/6-311G** + SO(BrO) ^a	-36.4	15
	Best theoretical value from literature	-25.2±1.5	See supplementary materials
	Average literature values	-25.0±2.1	See supplementary materials
(2) BrO + HO ₂ → HBr + O ₃	Experimental	-7.7	8
	BD(TQ)/CBS + SO(BrO) ^a	-4.3	This work
	CCSD(T)/6-311G** + SO(BrO) ^a	-7.7	15
	Best theoretical value from literature	-4.2(>±0.5)	See supplementary materials
	Average literature values	-7.1±3.3	See supplementary materials
(3) BrO + HO ₂ → OBrO + OH	BD(TQ)/CBS + SO(BrO) ^a	14.9	This work
	Best theoretical value from literature	17.1±2.0	See supplementary materials
	Average literature values	15.3±2.8	See supplementary materials
(4) BrO + HO ₂ → BrOO + OH	BD(TQ)/CBS + SO(BrO) ^a	5.9	This work
	Best theoretical value from literature	5.4±2.0	See supplementary

	literature		materials
	Average literature values	2.9±3.5	See supplementary materials

^a For BrO, the ground electronic state is $\tilde{X}^2\Pi$, and the experimental equilibrium spin-orbit (SO) state separation between the $\tilde{X}^2\Pi_{1/2}$ and $\tilde{X}^2\Pi_{3/2}$ states is 975.43 cm^{-1} (or 2.7889 kcal.mol^{-1}) (ref.32). Using this SO splitting, the $\tilde{X}^2\Pi_{3/2}$ SO state of BrO is lower than the unperturbed $\tilde{X}^2\Pi$ state by 1.39 kcal.mol^{-1} .

Table 7.

(a) Standard state enthalpy of activation (ΔH^\ddagger), standard state entropy of activation (ΔS^\ddagger) and standard state free energy of activation (ΔG^\ddagger) for channel 1(b), $\text{BrO} + \text{HO}_2 \rightarrow \text{HOBr} + \text{O}_2$ ($\tilde{\alpha}^1\Delta_g$) computed at the BD(TQ)/CBS//M06-2X/AVDZ level (incl.SO correction for BrO), at three temperatures 200, 298 and 400 K.

Temperature (K)	ΔH^\ddagger at $s=0 \text{ \AA}$ kcal.mol ⁻¹	ΔS^\ddagger at $s=0 \text{ \AA}$ kcal.mol ⁻¹ K ⁻¹	ΔG^\ddagger at $s=0$ kcal.mol ⁻¹	$(k_B T/hc^0)$ with $c^0=1$ cm ³ molecules ⁻¹ s ⁻¹
200	-3.0448	-0.11954	20.863	41.65 x10 ¹¹
298	-3.0438	-0.11989	32.683	62.06x10 ¹¹
400	-3.0428	-0.11993	44.929	83.33 x10 ¹¹

(b) Values of the terms in $\ln k = \ln(k_B T/hc^0) + \Delta S^\ddagger/k_B - \Delta H^\ddagger/(k_B T)$ (equ.3 in text) at 200, 298 and 400 K

Temperature (K)	$-\Delta H^\ddagger/k_B T$ at $s=0 \text{ \AA}$	$\Delta S^\ddagger/k_B$ at $s=0 \text{ \AA}$	$-\Delta G^\ddagger/k_B T$ at $s=0$ \AA	$(\ln(k_B T/hc^0))$
200	7.66186069	-60.15934433	-52.49748364	29.06
298	5.14053513	-60.33605095	-55.19551582	29.46
400	3.82839351	-60.35733161	-56.52893810	29.75

(c) Relative values of the terms $-\Delta H^\ddagger/(k_B T)$, $\Delta S^\ddagger/k_B$ and $\ln(k_B T/hc^0)$ at 200, 298 and 400 K taking the value at 400 K as zero in each case. These relative values are plotted against $1000/T$ in Figure 4.

Temperature (K)	$\Delta(-\Delta H^\ddagger/k_B T$ at $s=0$ $\text{\AA})$	$\Delta(\Delta S^\ddagger/k_B$ at $s=0 \text{ \AA})$	$\Delta(-\Delta G^\ddagger/k_B T$ at $s=0 \text{ \AA})$	$\Delta(\ln(k_B T/hc^0))$
200	3.8334671808	+0.197987273	4.03145	-0.69
298	1.3121416219	+0.021280657	1.33342	-0.29
400	0.0000000000	0.0000000000	0.00000	0.000

Table 8. Comparison of recommended experimentally derived rate coefficients (Atkinson et al., ref.(3)) for the BrO + HO₂ reaction in the temperature range 200-400 K , with computed values obtained in this work (cm³ molecule⁻¹s⁻¹)

Temp./K	Experimentally derived (3) k	k _{TST} ^(a) This work	k _{ICVT/SCT}	k _{overall,(ii)} calculated from equation (1) this work ^(b)
200	5.49x10 ⁻¹¹	6.64x10 ⁻¹¹	8.46x10 ⁻¹²	8.18x10 ⁻¹²
220	4.38x10 ⁻¹¹	3.43x10 ⁻¹¹	5.28x10 ⁻¹²	5.17x10 ⁻¹²
240	3.62x10 ⁻¹¹	2.00x10 ⁻¹¹	3.60x10 ⁻¹²	3.55x10 ⁻¹²
260	3.03x10 ⁻¹¹	1.28x10 ⁻¹¹	2.64x10 ⁻¹²	2.61x10 ⁻¹²
280	2.69x10 ⁻¹¹	8.85x10 ⁻¹²	2.04x10 ⁻¹²	2.02x10 ⁻¹²
298	2.40x10 ⁻¹¹	6.67x10 ⁻¹²	1.67x10 ⁻¹²	1.66x10 ⁻¹²
300	2.38x10 ⁻¹¹	6.48x10 ⁻¹²	1.64x10 ⁻¹²	1.63x10 ⁻¹²
320	2.15x10 ⁻¹¹	4.96x10 ⁻¹²	1.37x10 ⁻¹²	1.36x10 ⁻¹²
340	1.96x10 ⁻¹¹	3.95x10 ⁻¹²	1.17x10 ⁻¹²	1.16x10 ⁻¹²
360	1.80x10 ⁻¹¹	3.25x10 ⁻¹²	1.03x10 ⁻¹²	1.03x10 ⁻¹²
380	1.67x10 ⁻¹¹	2.75x10 ⁻¹²	9.16x10 ⁻¹³	9.13x10 ⁻¹³
400	1.53x10 ⁻¹¹	2.36x10 ⁻¹²	8.30x10 ⁻¹³	8.27x10 ⁻¹³

(a) See Table S5; TST values for k_{inner} computed with POLYRATE

(b) k_{outer} obtained from PST calculations with VARIFLEX and k_{inner} obtained from ICVT/SCT calculations with POLYRATE (values in column 4)

Figure Captions

Figure 1. Schematic pathways of the five channels (1a,1b,2,3,4) in the BrO + HO₂ reaction showing the stationary points with their relative electronic energies with zero-point correction at 0 K in kcal.mol⁻¹ at the BD(TQ)/CBS level (incl. SO correction for BrO) in brackets (note before ZPE correction RC(1b) is lower than TS(1b), but with ZPE correction RC(1b) is slightly above TS(1b)).

Figure 2. VMEP, Δ ZPE and VaG curves of channel 1(b) BrO + HO₂ → HOBr + O₂ ($\tilde{a}^1\Delta_g$) from POLYRATE calculations at the BD(TQ)/CBS//M06-2X/AVDZ level (incl. SO correction for BrO; energies are in kcal.mol⁻¹ with respect to separate reactants).

Figure 3. Computed (BD(TQ)/CBS//M06-2X/AVDZ incl. SO correction for BrO) k (cm³molecule⁻¹s⁻¹) (k_{inner} values) versus T (K) curves (upper) and $\log_{10} k$ versus $1000/T$ curves (lower) of channel 1(b) BrO + HO₂ → HOBr + O₂ ($\tilde{a}^1\Delta_g$) obtained at various VTST levels (TST, CVT, ICVT, TST/ZCT, CVT/ZCT, ICVT/ZCT, TST/SCT, CVT/SCT, and ICVT/SCT) using POLYRATE. As $k^{\text{CVT}} \sim k^{\text{ICVT}}$ and $\kappa^{\text{ZCT}} = \kappa^{\text{SCT}} = 1$, k^{CVT} , k^{ICVT} , $k^{\text{CVT/ZCT}}$, $k^{\text{ICVT/ZCT}}$, $k^{\text{CVT/SCT}}$ and $k^{\text{ICVT/SCT}}$ curves overlap with each other. Also, since $k^{\text{TST/CAG}} = k^{\text{TST/SCT}} = k^{\text{TST/ZCT}}$, only $k^{\text{TST/SCT}}$ is plotted.

Figure 4. Plots of $\Delta \ln k$, $\Delta(\ln(k_B T/hc^0))$, $\Delta(-\Delta H^\# / k_B T)$ and $\Delta(\Delta S^\# / k_B T)$ vs $1000/T$ of the channel (1b) BrO + HO₂ → HOBr + O₂ ($\tilde{a}^1\Delta_g$) obtained by using POLYRATE (see text). (The rate coefficients are k_{inner} values).

In this figure, $\Delta \ln k = \ln k - \ln k|_{T=400\text{K}}$, $\Delta(-\Delta H^\# / k_B T) = -\Delta H^\# / k_B T + \Delta H^\# / k_B T|_{T=400\text{K}}$, $\Delta(\Delta S^\# / k_B T) = -\Delta S^\# / k_B T + \Delta S^\# / k_B T|_{T=400\text{K}}$ and $\Delta(\ln(k_B T/hc^0)) = \ln(k_B T/hc^0) - \ln(k_B T/hc^0)|_{T=400\text{K}}$ where # refers to TS and k refers to k^{TST} . All calculations are based on the BD(TQ)/CBS//M06-2X/AVDZ potential energy surface (incl. SO correction for BrO) (see Table 7).

Figure 5. Computed (BD(TQ)/CBS//M06-2X/CBS incl. SO correction for BrO) and experimental (2,5-9,11,12) k (cm³molecule⁻¹s⁻¹) versus T (K) curves (upper) and $\log_{10} k$ versus $1000/T$ curves (lower) of channel 1(b) BrO + HO₂ → HOBr + O₂ ($\tilde{a}^1\Delta_g$).

k_{overall} values are evaluated from equation (1) with

- (i) k_{outer} from PST (VARIFLEX) and k_{inner} from E,J-TST(VARIFLEX) and
- (ii) k_{outer} from PST (VARIFLEX) and k_{inner} from ICVT/SCT (POLYRATE).

Also plotted are k_{inner} values (k_{TST} and $k_{\text{ICVT/SCT}}$) from POLYRATE (see text).

The k_{inner} ($k_{\text{ICVT/SCT}}$) and k_{overall} (ii) plots are superimposed in this figure

Figure 6. Computed (BD(TQ)/CBS//M06-2X/CBS incl. SO correction for BrO) and recommended experimental k ($\text{cm}^3\text{molecule}^{-1}\text{s}^{-1}$) values from ref.(3) versus T (K) curves (upper) and $\log_{10}k$ versus $1000/T$ curves (lower) of channel 1(b) $\text{BrO} + \text{HO}_2 \rightarrow \text{HOBr} + \text{O}_2$ ($\tilde{\alpha}^1\Delta_g$). The values shown in Table 8 were used for this plot. For the k_{TST} plot (red curve), the TST rate coefficients for k_{inner} were computed with POLYRATE, see Table S5. For the $k_{\text{overall(ii)}}$ plot (blue curve), the $k_{\text{overall(ii)}}$ values were obtained from k_{outer} from PST calculations with VARIFLEX and k_{inner} from ICVT/SCT calculations with POLYRATE; see Table S7

Figure 1.

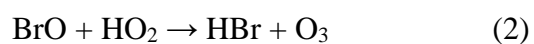
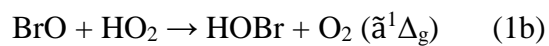
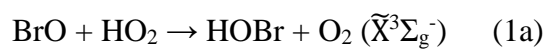
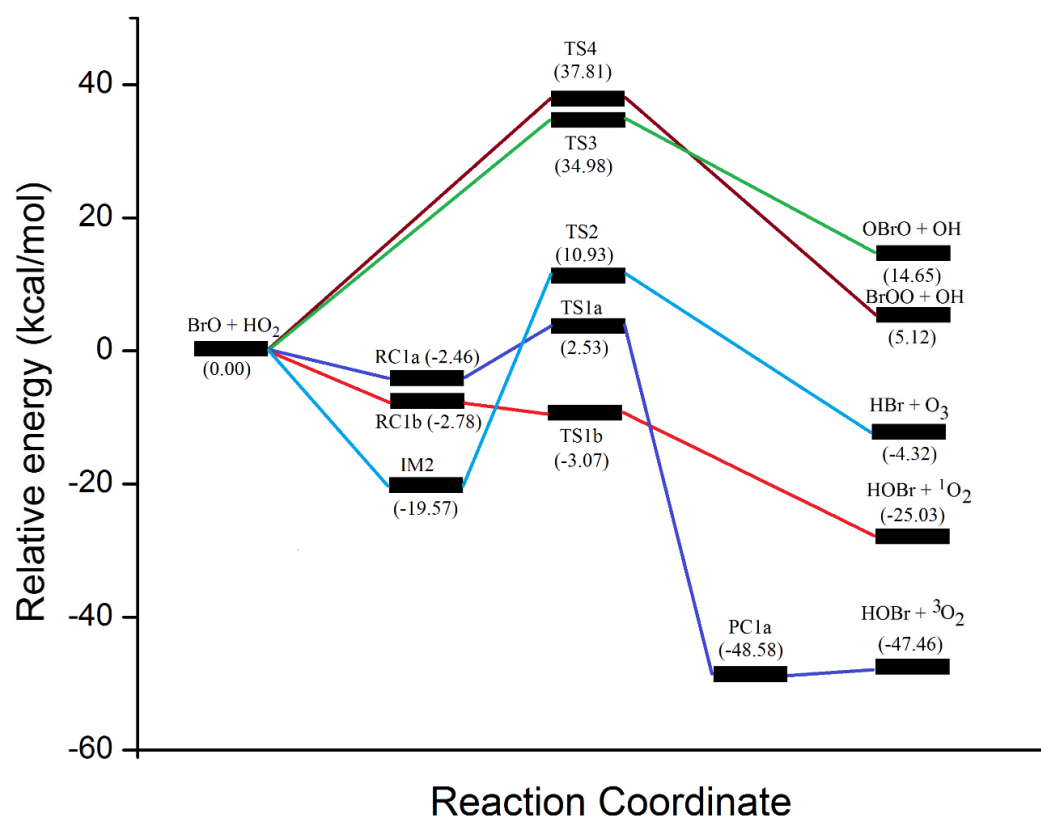


Figure 2.

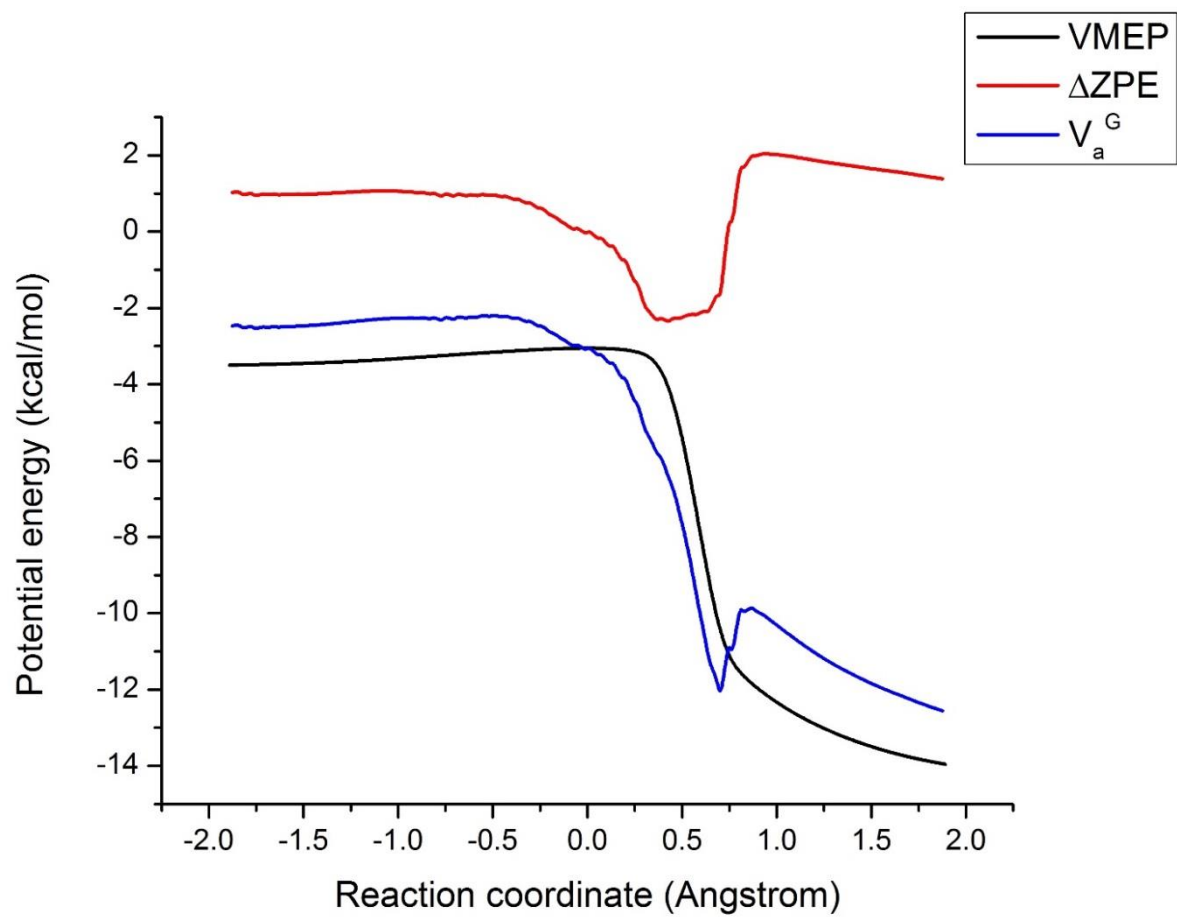


Figure 3.

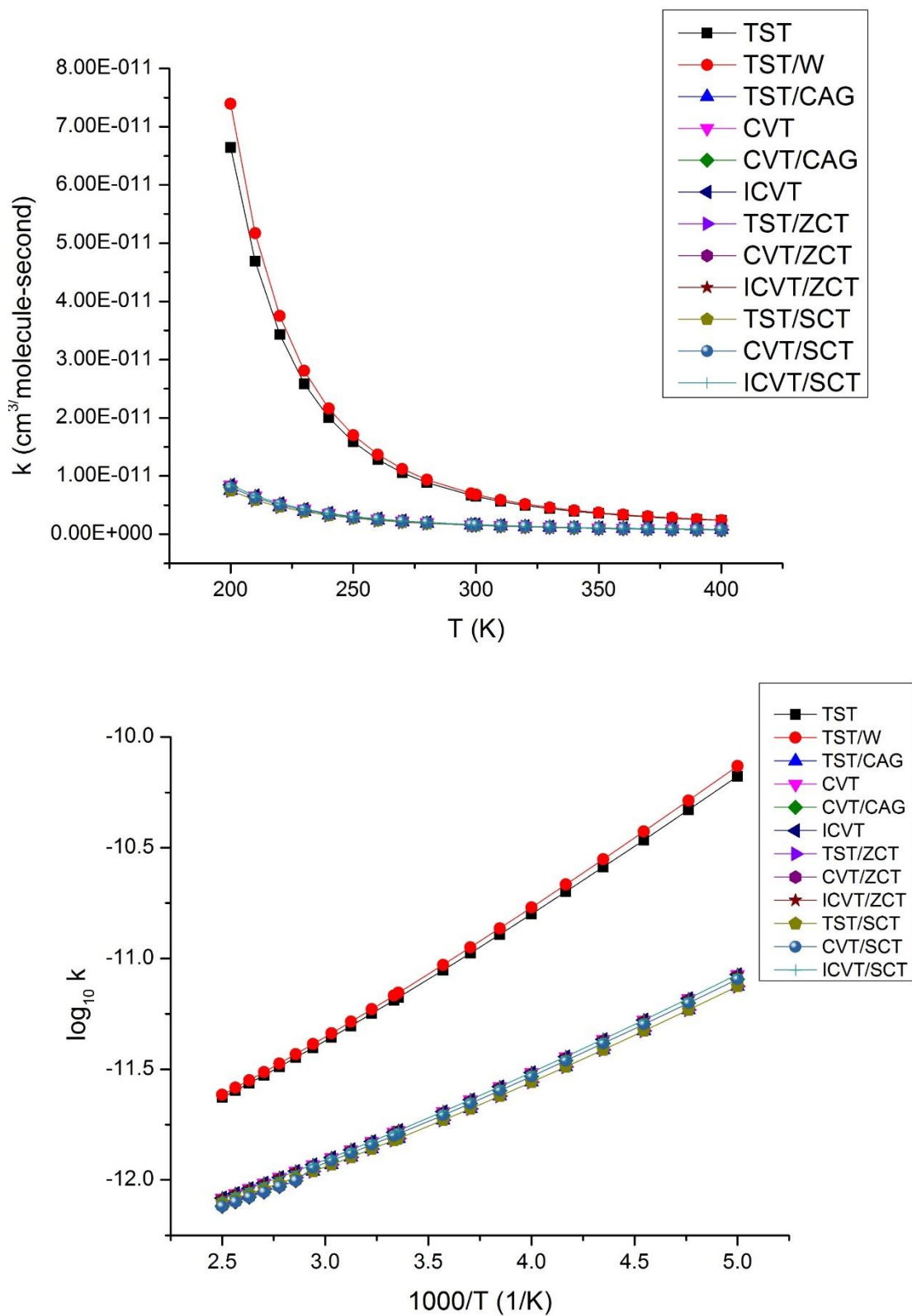


Figure 4.

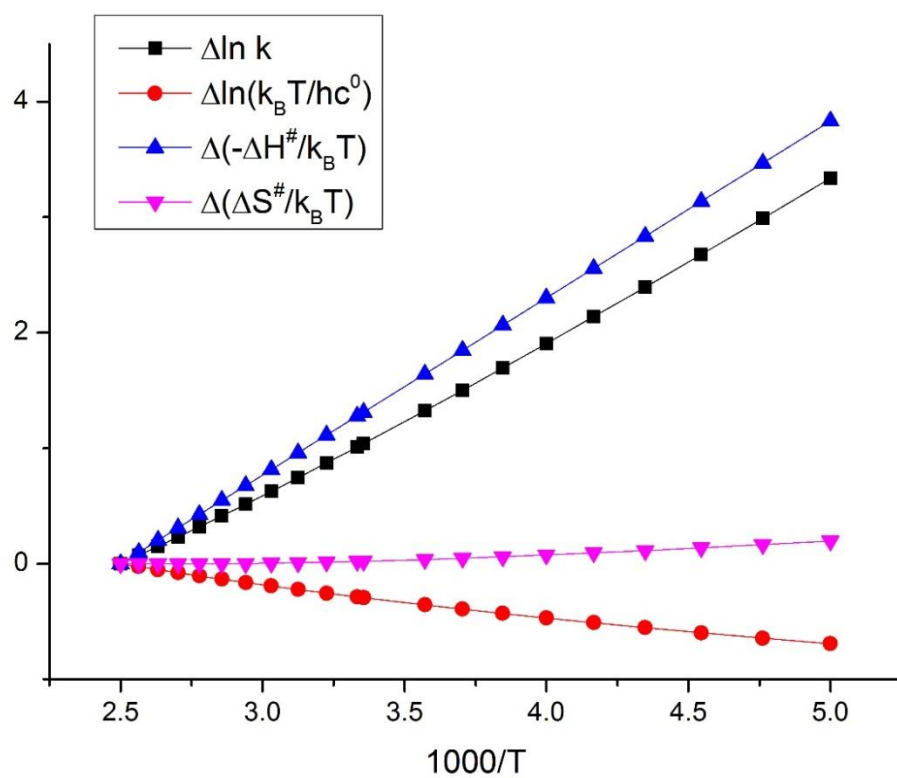


Figure 5.

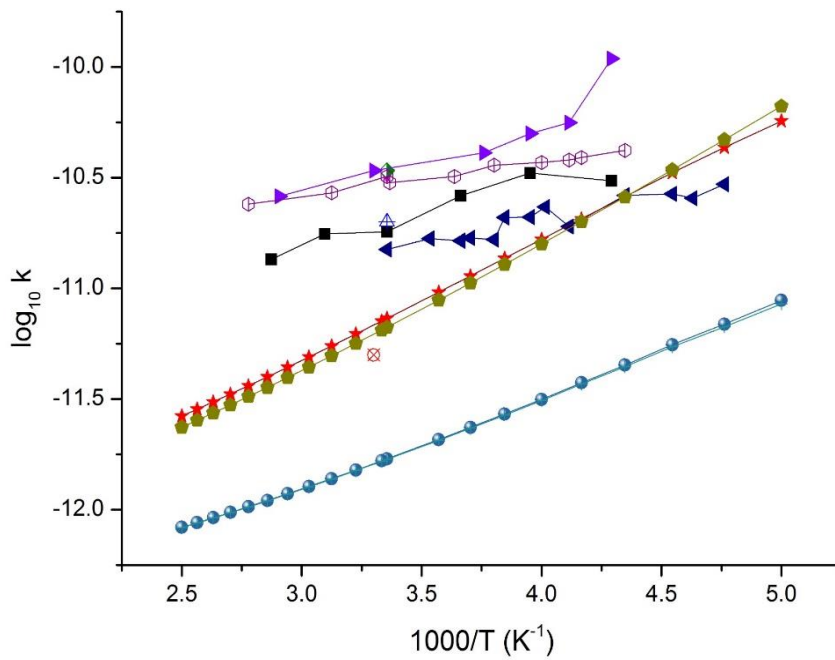
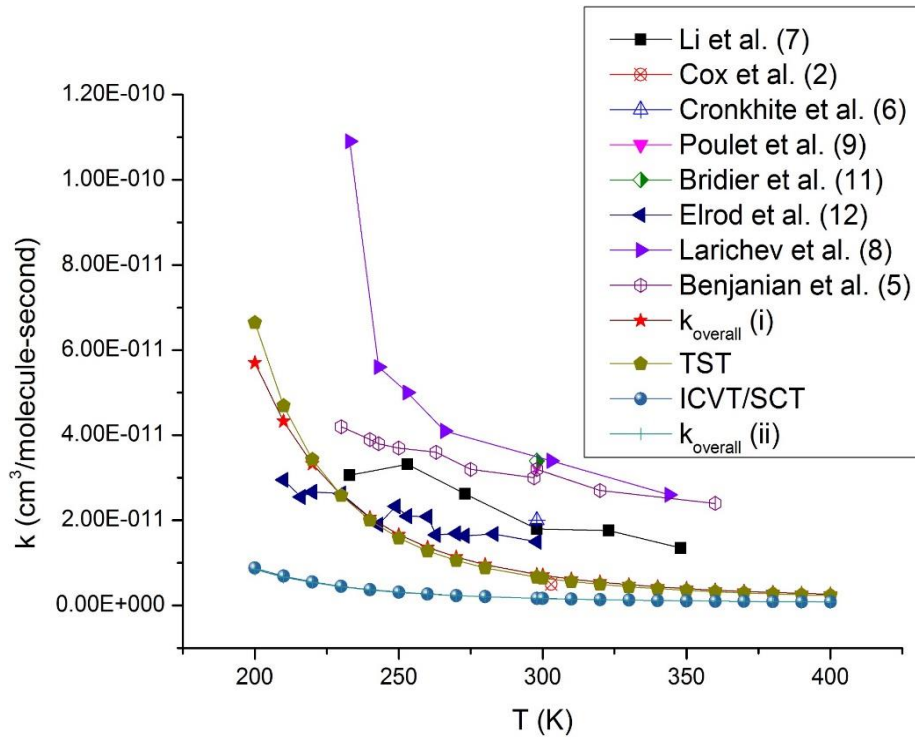


Figure 6.

